NTNU

Norwegian University of
Science and Technology

Comparing the caveolae mediated endocytosis of two DNA-chitosan polyplexes

Oladayo Folasire

Medical Technology
Submission date: July 2011
Supervisor: Catharina de Lange Davies, IFY

Norwegian University of Science and Technology
Department of Physics

Faculty of Natural Science and Technology
Department of Biotechnology

NTNU
Norwegian University of
Science and Technology

Master's thesis

Folasire Seun Oladayo

Thesis started: 01.02.2011
Thesis submitted: 08.07.2011

Discipline: Medical Technology: Medical Biotechnology

Title: *"Comparing the caveolae mediated endocytosis of two DNA-chitosan polyplexes"*

This work has been carried out at the Department of Physics, Norwegian University of Science and Technology, under the supervision of Catharina Davies de Lange.

Trondheim, 08.07.2011

Catharina Davies de Lange

Responsible supervisor

Professor at Department of Physics

Comparing the caveolae mediated endocytosis of two DNA-chitosan polyplexes

Folasire Seun Oladayo

Abstract

Understanding intracellular processing of gene vectors will help to improve vector design in gene therapy. Chitosan nanoparticles have been previously identified as safe and non toxic gene vector. Linear chitosan oligomer (LCO) and self branched trisaccharide chitosan oligomer (SBTCO) have been shown to be able to pack DNA, balancing between complexation and intracellular unpacking . However, the transfection efficacies of these two chitosans differs considerably with the level of transgene expression higher for SBTCO compared to LCO. SBTCO have been recently reported to be taken up solely by caveolae mediated endocytosis (CvME) while LCO uses both clathrin mediated endocytosis (CME) and CvME.

In the present study, the CvME was studied. An immunostaining protocol for detection of caveolin (cav) was established. Polyplexes of SBTCO seemed to trigger the formation of more caveosomes than did LCO polyplexes. SBTCO polyplexes were more localised in the caveosome than LCO polyplexes at 3 hours incubation period. These findings suggested that SBTCO polyplexes delivers more DNA into the cell than LCO polyplexes and that SBTCO polyplexes are processed intracellularly solely via the CvME pathway. Likewise, it suggested LCO polyplexes have preferred intracellular processing pathway which is not CvME. Collectively, these results demonstrated that SBTCO is protected from the degradative endosome and might therefore be an efficient and good tool to deliver therapeutic DNA.

Acknowledgments

I would like to thank Professor Catharina Davies de Lange, my supervisor, for her suggestions and constant support. I am also thankful to Astrid and Nina for their guidance through the imaging problems and challenges. Thanks to all workers in the department of biophysics, especially Kristine and Sabina, that contributed in one way or the other. Kristine helped in the laboratory, while sabina made enough chitosan for my use. I appreciate you all.

I cannot forget all my friends; the Spirit, Jare J. and Future, that made this journey possible. You stood by me during hard times, giving me the drive to keep on going. Finally, I appreciate my family members; Alice-Taiwo (the great mother), Lekan, Nike and Sade. I am privilege to share same blood with you.

All glory, honour and adoration be unto the Alpha and Omega, the beginning and the end, He who knows the end from the beginning, omnipotent and omniscience, GOD of host, for the completion of this masters programme.

Trondheim, Norway — Folasire Seun Oladayo

July 8, 2011

To Mrs Folasire Alice Taiwo and Late Folasire Isaac Adelere

Contents

List of abbreviation

A/P Amino-phosphate ratio.

AAM $2-acetamido-2-deoxy-D-glucopyranosyl-\beta-(1-4)-2-acetamido-2-deoxy-D-glucopyranosyl-\beta-(1-4)-2,5-$ anhydro-D-mannofuranose

Alexa555-sAb Alexa 555 labeled secondary antibody

bp Base pairs

cav Caveolin

CCP Clathrin Coated Pits

CCV Clathrin coated vesicle

CME Clathrin Mediated Endocytosis

CTB Cholera toxin subunit B

CvME Caveolae Mediated endocytosis

DDA Degree of deacetylation

DIC Differential interference contrast

DMEM Dulbeco‘s Modified Eagle‘s Medium

DNA Deoxyribonucleic acid

eNOS Endothelial nitric oxide

ER Endoplasmic Reticulum

GA Golgi Apparatus

HBSS Hank‘s buffer saline solution

LCO Linear chitosan Oligomer

MC Manders coefficient

MHC Major histocompatibility complexe

MP Macropinocytosis

Mwt Molecular weight

NA Nucleic acid

pAb Primary antibody

PAMPS Pathogen associated molecular patterns

PC Pearson‘s coefficient

RME Receptor Mediated endocytosis

ROI Region of Interest

sAb Secondary antibody

SBTCO Self branched trisaccharide chitosan oligomer

SD Standard deviation

TGN Trans golgi network

List of Figures

List of Tables

Chapter 1

Introduction

Gene therapy can give a lasting solution to both genetic and non genetic disease. Although gene delivery is promising, the problem of ineffective delivery of the genetic material limits it applications. For a successful gene therapy, the gene must be delivered to the target site which could either be cytoplasm or nucleus depending on the reason for therapy. Naked nucleic acid (NA) are easily degraded by cytoplasmic nuclease. If not, they would have been the best option for non cytotoxic delivery. This is because there would be no need for putting them into a carrier which could be toxic to the host cells. Other factors such as large macromolecular size and surface charges also limits the use of naked NA in gene therapy. In order to overcome these limitations, researches are being carried out on effective carriers for the NA. These carriers are classified as either viral or non viral. Viral vectors such as adenovirus, adeno-associated viruses (AAV) achieves an effective transfection. The main set back of viral vectors are their safety issues [1]. This ultimately led to use of non viral vectors such as bio-polymers in gene delivery [2]. Chitosan, a natural polysaccharide derived from chitinous exoskeleton of crustacean, insect and cell wall of fungi have a promising properties which could be harness in gene therapy [3].

At the department of biotechnology Norwegian University of Science and Technology (NTNU), a derivative of chitosan, self branched trisaccharide chitosan oligomer (SBTCO) with improved physio-chemical properties was curtailed by Strand et al. [4]. SBTCO balances polyplexe unpacking and DNA release. SBTCO achieves higher transfection compare to linear chitosan oligomer (LCO). SBTCO polyplexes cellular uptake was demonstrated to be solely via caveolae mediated endocytosis (CvME) while LCO polyplexes were taken up by both clathrin mediated endocytosis (CME) and CvME (unpublished result). This suggested that caveolin (cav) containing intracellular organelles (caveosomes) might be involve in the intracellular transport of SBTCO polyplexes and some LCO polyplexes. After the uptake of the polyplexes by the cav positive membrane domain (caveolae), the membrane domain pinches off to form the cav positive vesicle (caveolar) which fuses with the cav positive organelle (caveosome). In this work, all cav positive intracellular structures

will be refer to as caveosomes. The uptake of SBTCO via CvME suggested that caveosome might be responsible for protecting the DNA cargoed by SBTCO and this might be responsible for higher transfection triggered by SBTCO polyplexes [4].

Although the high transfection achieved by SBTCO has been established [4], the intracellular processing pathway is yet to be clarified. The knowledge of intracellular processing and fate of SBTCO polyplexes will give a better understanding of mechanism by which SBTCO-DNA polyplexes achieved high transfection over LCO-DNA polyplexes. The purpose of the present work is to compare the uptake of SBTCO and LCO polyplexes and relate them to caveosome. This will help to know the intracellular processing pathway of these polyplexes in relation to CvME. HeLa cells were incubated in the polyplexes for 15 minutes, 1 hour and 3 hours so as to show the kinetics of these polyplexes intracellularly. Likewise, polyplexes were colocalised with caveosomes.

Counting of intracellular DNA and caveosomes were carried out. The number of intracellular DNA explained the uptake of the polyplexes. It also clarified whether DNA are being protected from degradation. The number of caveosomes explained whether the caveosome organelle are fully or partially involved in polyplexes intracellular processing. The mean volume and total volume of DNA and caveosomes were also analysed. The mean and total volume of DNA described the size of the intracellular DNA particle while the mean and the total volume of the caveosomes described the average and total size of the caveosomes. The size of the caveosomes showed whether the polyplexes are located in them thereby being protected from the degradative pathway. It also showed whether the polyplexes are stored for a while before being released at their final destination. Finally, the colocalisation analysis showed the location of these polyplexes, whether they are in the caveosomes or not.

Chapter 2

Theory

2.1 Gene Vectors

Gene therapy, the transmission of NA into target cells or organs is a promising therapy. It could be the magic bullet being expected as the final solution to pathological conditions. Although gene therapy is promising, it is limited by inefficient gene delivery and transfection. Uptake by the cell, intracellular processing and delivery into the cytosol or nucleus are factors to be considered in order to achieve effective transfection. Uptake of naked DNA by the cell is limited by several factors. The negative charge phosphate backbone of DNA opposes the negative charges on the plasma membrane. Also, cytosolic nucleases degrades DNA thereby reducing the transfection efficiency. This has led to design of carriers for the DNA which can help in efficient delivery [3]. In the search for an effective carrier, many materials have been developed, they are classified as viral or non viral carriers [3].

2.1.1 Viral mediated gene delivery

Virus such as adenovirus, lentivirus and AAV have proven to transfect cells efficiently. Viral vectors are known for high transfection in gene delivery though they poses safety issues [3]. Issues such as bio-incompatibility, oncogenicity, activation of other viral particles insitu etc have been reported. This therefore call for use of non-viral vectors to fulfil the need for a safe and efficient gene delivery [5].

2.1.2 Non-viral mediated gene delivery

Non viral delivery is basically classified into physical and carrier mediated delivery. The physical methods involves the use of ultrasound, gene gun, electroporation etc to enhance

gene delivery into cells [6]. The other method involves the use of carriers to transport the gene in order to achieve an efficient gene delivery. Cationic lipids and cationic polymers are major classes of this non viral carriers [3]. Cationic lipids are positively charged amphiphile made of three basic component; the polar head group, hydrophobic moiety (steroid or alkyl chains) and linker [7, 8]. The polar head is positively charged due to protonation of amino groups which are usually amine, amidine, guanidium, pyridinium etc. Optimal performance of cationic lipid carrier depends on the hydrophobic domain and the linkers. Example of cationic lipids are N-(1-(2,3-dioleyloxy)propyl)-N,N,N-trimethylammonium chloride (DOTMA) and dioctadecylamido-glycylspermine (DOGS) [8].

Cationic polymers like poly(D,L-lactic acid), gelatin, alginate and chitosan differ from cationic lipids in several aspects such as chemical structure, interaction with DNA and intracellular behaviour [7]. Cationic polymers are able to condense large genes into smaller structures and to mask negative DNA charges. Cationic polymers do not contain a hydrophobic moiety and they are soluble in water [7]. Another advantages of cationic polymers is their easy to modify and synthesise characteristics. Their length, functional groups, geometry and flexibility could be modulated to achieve a desired characteristic. They also adsorb or encapsulate oligonucleotides or gene optimally [7].

Cationic lipids -DNA complexes (lipoplexes)

Complexes between cationic lipid and DNA can be prepared by simple mixing of cationic lipids and DNA in an aqueous solution. This complexes are stabilised by electrostatic interaction between the positively charged lipid head group and negatively charged phosphate group of the DNA backbone. The size of lipoplexes formed is a function of the charge of the lipid-DNA. At neutral charge, lipoplexes are usually larger and may precipitate while at higher positive or negative charge the lipoplexes are usually smaller in diameter and size [7].

Cationic polymer-DNA complexes (polyplexes)

Polyplexes are formed by mixing DNA with cationic polymer or vice versa. Polyplexes have more advantages over lipoplexes in that they compact DNA more efficiently which enhances cellular uptake via endocytosis [7]. Compaction by polyplexes protects DNA from nuclease damage. It depends on the charge ratio i.e, molar ratio of positive charge of cationic polymer to the negative charge of the DNA phosphate group (A/P ratio) [9]. At a high A/P ratio, polyplexes are positively charged, small and with high solubility. Polyplexes with high A/P ratio also interact with cell surface directly due to the presence of negatively charged cell-surface molecules like proteoglycans [9].

Chitosan

Chitosan is a natural, non synthetic, biodegradable and non toxic polysaccharide. It is biocompatible with soft tissue and this characterise its usage in medical applications [3]. Chitosan is obtained by alkaline de-acetylation of chitin which is the structural element

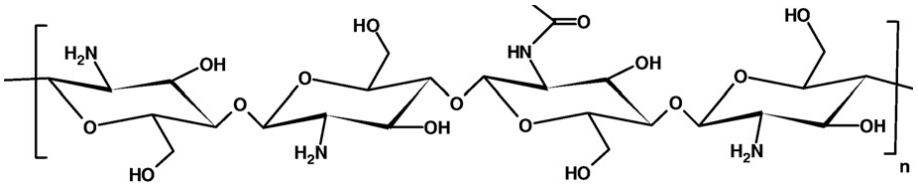

Figure 2.1: The chemical structure of chitosan biopolymer. The figure shows the repeating units, acetylated and de-acetylated monomer of chitosan . These are the D-glucosamine and N-acetyl-D-glucosamine units, linked via $(1 \rightarrow 4)$ glycosidic bonds. Chitosan is a natural biopolymer derived from the chitinous exoskeleton of crustaceans, insect. It is also derived from fungi cell wall. Adapted from Mao et al. [3].

in the exoskeleton of crustaceans, insects. Chitosan is also found in cell walls of fungi [9]. It is composed of randomly distributed $\beta-(1-4)$-linked D-glucosamine and N-acetyl-D-glucosamine as shown in Figure 2.1. Chitosan binds tightly to DNA due to it polycationic character [3, 10].

Chitosan is soluble in acids such as acetic acid, citric acid etc and insoluble at neutral and alkaline pH values. This is because at acidic pH, the primary amines in the chitosan backbone become positively charged. These protonated amines enable chitosan to bind to negatively charged DNA by electrostatic interaction [11]. The solubility of chitosan is also influenced by the degree of de-acetylation (DDA), molecular weight (Mwt) and ionic strength of the solution. Encapsulation efficiency of DNA by chitosan increases as the DDA increases [3]. Very high DDA chitosan forms a stable and inefficient complex which do not dissociate from DNA fast enough to stimulate transfection. This call for the need to balance between polyplexes stability, DNA protection and polyplexes dissociation in the cytosol [12]. Chitosans are used in applications such as gene delivery, pharmaceutical, wound dressing and edibles.

LCO and SBTCO

LCO and SBTCO, modifications of chitosan were curtailed by Strand group [4]. LCO is produce by nitrous acid depolymerization of fully de-acetylated chitosan ($FA < 0.002$). SBTCO is produced from fully deacetylated chitosan, simultaneously self branched and substituted with trisaccharide, $2-acetamido-2-deoxy-D-glucopyranosyl-\beta-(1-4)-2-acetamido-2-deoxy-D-glucopyranosyl-\beta-(1-4)-2,5-$ anhydro-D-mannofuranose (AAM) [4, 13]. SBTCO forms polyplexes of high colloidal and physical stability at physiological pH. SBTCO has a higher solubility due to the branches and functional glycosyl group AAM [2]. It forms globules of larger height as a result of steric hindrance within its structure which helps in actualising an efficient gene delivery [4, 12, 13].

Comparing the relative amounts of transfected cells at different time of incubation, SBTCO exhibited more rapid onset of transgene expression than LCO [4]. The transfection achieved by SBTCO is 10 times higher than transfection achieved by LCO polyplexes. The high transfection was associated to high gene loading capacity and ability to target lectin on cell membrane using AAM [2, 4]. Transfection efficiency of SBTCO has created more interest; elucidating the intracellular processing of this polyplexes will be of relevance to it clinical application in gene therapy. The difference in LCO and SBTCO is shown in Figure 2.2 and Figure 2.3.

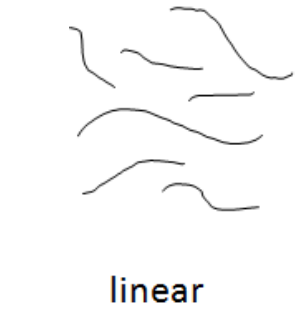

Figure 2.2: Schematic representation of LCO. LCO is produced from fully deacetylated chitosan. LCO is neither branched nor modified with glycosyl group. Adapted from Strand et al. [4].

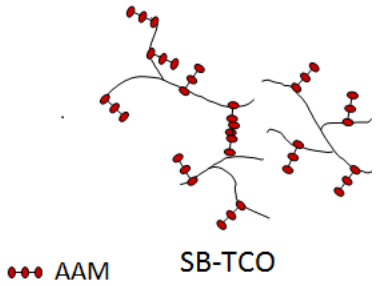

Figure 2.3: Schematic representation of SBTCO. Chitosan oligomers are fully deacetylated, self branched and functionalised with AAM. The red dots represents the AAM groups used to functionalise the SBTCO. Adapted from Strand et al. [4].

2.2 Endocytosis

Cells take up molecules from their surrounding media using various uptake mechanisms. These mechanisms lead to intracellular processing pathways which ultimately determine the fate of these molecules. Cell binding usually precedes the uptake of the molecules and the negative charge of the cell membrane has been implicated. Molecules have been reported

to bind to proteoglycan cell component such as heparan sulfate, chondroitin sulfate so as to be taken up by the cell [7]. Cell bound, surface adsorbed or receptor bound cargoes are usually taken up by different mechanism of endocytosis which include phagocytosis (cell eating) and pinocytosis (cell drinking).

Some of the endocytic pathways uses molecular machinery such as dynamin, actin cytoskeleton etc during the process of uptake [14, 15]. Dynamin is a modular 100kda protein that hydrolyses guanosine triphosphate (GTP) to guanosine diphosphate (GDP) and organic phosphate (Pi) (GTPase) [16]. CvME, CME and some clathrin and caveolin independent endocytosis (CLIC) uses dynamin to liberate membrane budding. Dynamin also serves as mechanochemical or regulator of cargo uptake. Dynamin is found around the neck region of caveolae where they pinch caveolae off the membrane [14, 15]. They are activated by hydrolysis of GTP and upon the hydrolysis, they undergoes a change in conformation into an uncoiled protein structure. This uncoiled protein generates a force that severs the bud neck and ultimately leading to the pinching off of the membrane bud. They also recruits other proteins such as lipid modifying enzymes. These enzymes seals the neck of the vesicles after pinching off [17].

2.2.1 Phagocytosis

Phagocytosis literally means cell eating. It is used by specialised cells such as neutrophils, tissue macrophages and blood monocytes to engulf large particles such as bacteria [6, 17, 18]. Phagocytes can eat particles that are bigger than them. This is accomplished by the formation of a pseudopodia through which the particles are taken up. Following the uptake, the pseudopodia closes to form the phagosome which later matures into phagolysosomes by fusing with lysosomes. Inside the phagolysosomes, the uptaken particles are digested [6, 17, 19].

2.2.2 Pinocytosis

Pinocytosis simply means cells drinking. It is classified into four morphologically distinct pathways which are discuss below;

Macropinocytosis (MP)

Macropinocytosis (MP) involves large endocytic vesicles of irregular size and shape. It is generated by actin-dependent process. MP is stimulated by growth factors or phorbol esters which leads to formation of membrane ruffling [6]. The ruffle fuses with plasma membrane to form macropinosomes, a large endocytotic vesicle that recycle back to the membrane surface it content [6]. Macropinosomes size is around 5 μm. MP helps dendritic cells to sample large volume of extracellular content. Proteins internalized via MP in dendritic cells can be processed and presented on major histocompatibility complexe class

II (MHC class II) [6, 16].

Clathrin mediated endocytosis (CME)

Clathrin mediated endocytosis (CME) is the best characterised endocytic mechanism. It is a constitutive mechanism of pinocytosis in mammalian cells [6, 16]. It carries out continuous uptake of essential nutrients, pathogens, antigens and growth factors [6]. It is initiated by the formation of clathrin coated vesicle (CCV). The main component of CCV is a three legged protein triskelion known as clathrin which interacts to form the polyhedral lattice surrounding the CCV. Ligands binds receptors in the clathrin coated pit (CCP) to form

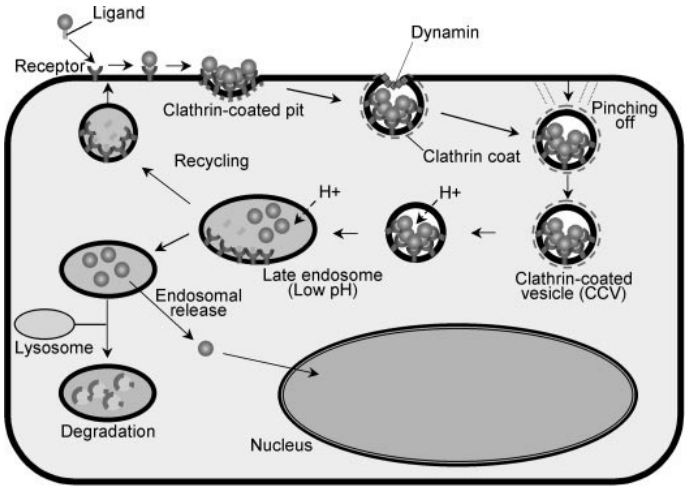

Figure 2.4: A schematic diagram showing the uptake mechanism and intracellular processing of cargo via CME. Ligands can either bind to the receptors to enter the cell by receptor mediated endocytosis (RME) or can be taken up by adsorption. Clathrin coated pit (CCP) accumulates cargo and pinches off with the help of dynamin protein. The cargo is transported to early endosome for sorting. Receptors may be recycled for another round of uptake. Unrecycled ligands are further transported to the late endosomes. Late endosome fuses with lysosome to initiate digestion of cargo. Cargo that escape the endosome are released into the cytosol and in the case of gene it might enter the nucleus to trigger transfection. Adapted from Khalil et al. [6].

the receptor-ligand complex which then associates with adaptor protein AP2. Association of receptor-ligands with AP2 is followed by pinching off of the bud and this process of pinching off is carried out by dynamin protein [6, 16]. Cargo internalise via CME are delivered to the early endosome for sorting and recycling of membrane receptor proteins. Early endosomes matures into late endosome and late endosomes can either undergo homotypic fusion with another late endosome or undergo heterotypic fusion with lysosome [19]. The uptake process and intracellular trafficking via CME is described in Figure 2.4.

CME has been implicated in uptake of transferrin from the cell environment by the transferrin receptor (TFR) [16]. This type of uptake is know as receptor mediated endocytosis (RME) and it can enable membrane impermeant nanoparticles to enter target cells.

Caveolae mediated endocytosis (CvME)

Caveolae mediated endocytosis (CvME) is a non constitutive cellular mechanism of cargo uptake. Molecules taken up via CvME are assembled and concentrated in the lipid rich, detergent resistant, cav containing caveolae [20]. Caveolae domain on cell membrane are involve in cholesterol homeostasis. The caveolae are best characterised lipid raft found on the membrane as a stable flask shaped invaginations [20, 21, 22]. They are characterised by distinct lipid concentration such as sphingolipid and glycolipid and are sensitive to cholesterol depletion [21, 22]. Caveolae are partially immobile at the plasma membrane and their endocytosis requires a stimulus such as a ligand binding [20].

Caveolae domains are stable with low rate of turnover. They buds in response to phosphorylation. Signalling molecules such as endothelial nitric oxide (eNOS) concentrate in them. There, eNOS is bound to the scaffolding domain as shown in Figure 2.5. Ligands triggers

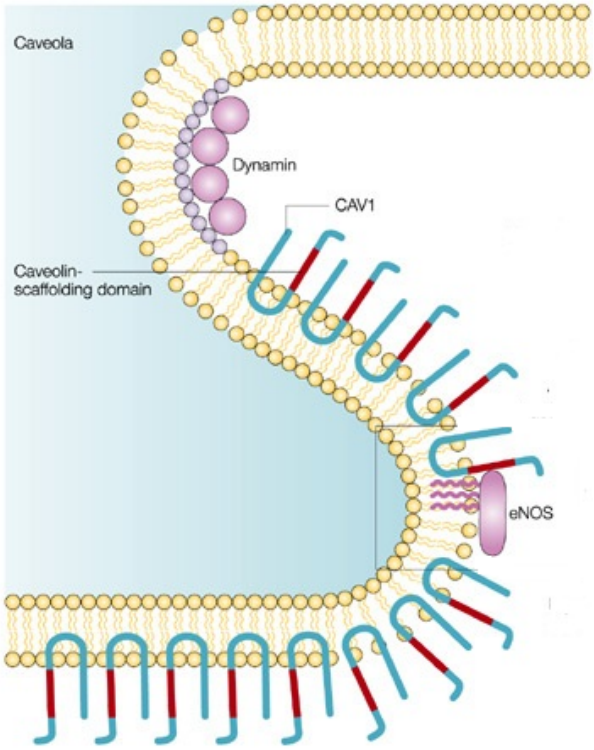

Figure 2.5: A schematic diagram of caveolae. eNOS: Endothelial nitric oxide synthase. The caveolin protein spans the membrane as a hairpin loop with both N and C terminal in the cytosolic side. The N terminal is responsible for oligomerisation of the protein and targeting of the caveolin to the membrane after synthesis. This terminal also harbors the scaffolding domain which is actively involve in signalling. Adapted and modified from Carver et al. [24].

caveolae internalisation, and example of such ligands are albumin, bacteria, SV40 viral particle and cholera toxin subunit B (CTB) [14, 15]. These ligands binds specific receptors in the caveolae. Receptor such as gp60, CD48, MHC class I and gangliosides (GM1) have

been reported to be located in caveolae [14, 15]. Function of caveolae has been describe as;

1. Scaffold for signalling events ; signalling proteins, growth factors receptors, G-proteins, nitric oxide synthase are located in caveolae.
2. Buffer regulating plasma membrane lipid composition [23].

Caveolae mediates either degradative endocytic pathway or non degradative endocytic pathway as illustrated in Figure 2.6. The degradative pathway, although differs from CME

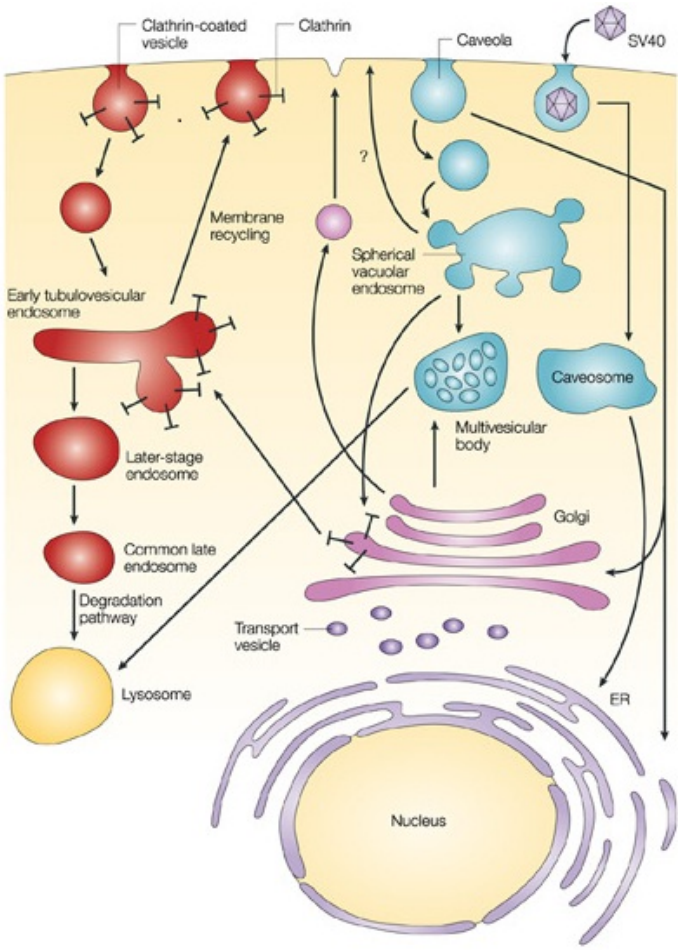

Figure 2.6: A schematic diagram of uptake, intracellular trafficking of molecules and link between CME and CvME pathways. Left pathway(CME) and Right pathway (CvME). Adapted from Carver et al. [24].

in the earlier stages, it meets with CME cargoes in the endosomes [14, 24]. In the non-degradative pathway, ligands in the caveolae are transported and delivered to a different intracellular compartment which is totally different from endosomes known as caveosomes. Endoplasmic reticulum (ER) and golgi apparatus (GA) have been reported to be endpoint of these ligands [14]. Based on this, caveolae domain has been suggested to contain two

different type of cargoes which can be targeted to different organelles leading to different fate [14, 25, 26].

Endocytosis and budding of caveolae membrane leads to formation of intracellular vesicle called caveolar. Caveolar are cellular structures that buds from the caveolae membrane domain. Caveolar fission from the plasma membrane is inducible by actin cytoskeleton, GTPases such as dynamin, protein kinases etc. Caveolar fission from the membrane is tightly regulated which is the reason why it processes different surface ligand. After the budding of the caveolar, they are released into the cytoplasm where they can merge or release their cargo into endosome vesicles. Alternatively, caveolar can fuse with caveosomes and release it cargo. Inside the cells, caveolar are continuously docking and fusing with these two endocytic compartment [27].

Caveosomes are cav positive, neutral pH organelle rich in cholesterol and glycosphingolipids [20]. caveosome can protect cargo from hydrolytic degradation. SV40 virus has been reported to remain in the caveosomes for several hours after caveolar fuses with the caveosomes. They are later sorted by tubular cav negative carriers that move along the microtubule to endoplasmic reticulum (ER) [20].

Caveolin (cav)

caveolin (cav) proteins are 21-24 kDa integral membrane proteins found in caveolae, caveolar and caveosomes. They forms a loop in the membrane with both N and C terminal in the cytosol as shown in Figure 2.5 [15, 25, 28]. They exist as three isoforms, which includes cav-1 (α, β), cav-2 (α, β, γ) and cav-3.

Cav-1 and cav-2 form heteropolymer and are found in many cell types such as adipocyte, fibroblast and endothelial cells. In contrast, cav-3 form homopolymer and is present only in muscle cells [22, 23, 29, 30].

In summary, different endocytic pathways have their specific characteristics, ligands, receptors and molecule size that are taken up, this is summarised in Table 2.1.

Table 2.1: Characteristics of some selected endocytosis pathways.

Endocytic pathways	size range	receptors	ligands
Phagocytosis	≥ 0.5 μm [18]	Fc and CD44	Ab, PAMPS [31]
MP	$1 - 5\mu m$ [6]	-	TAT ligands
CME	100-150nm	TFR	Transferrin [16]
CvME	50-100nm [16]	GM1, gp60, CD48 [14]	SV40, CTB [14, 26]

Fc: fragment crystallisable region, Ab: antibody, PAMPS: pathogen associated molecular patterns, TAT: trans-activating transcriptional activator, TFR: transferin receptor, GM1: gangliosides, gp: glycoprotein, SV: simian virus, CTB: choleratoxin subunit B and CD: Human Cell Differentiation.

2.3 Endosomal escape of cargoes

In order to achieve a higher transfection, DNA must escape endosome which contain hydrolytic enzymes for degrading it content. Some cationic lipids have potential of escaping the endosome by membrane fusion or lipid mixing activity. In contrast, cationic polymers cannot fuse or destabilise the endosome by direct interaction with the endosomal membrane. Although, polymers such as polyethylineimine (PEI) have intrinsic property to escape the endosomal degradation by proton sponge effect, chitosan can not. Proton sponge effect explains how endosome rupture as a result of swelling. Buffering capacity of the polyamines causes accumulation of chloride ion which induces swelling and lysis of the endosome [13]. An alternative method of releasing cargo from endosomes is photochemical internalisation technology (PCI) [32]. PCI uses light and a photosensitiser to trigger endosomal rupture. Since chitosan do not have the capability to disrupt or escape the endosome, targeting the non degradative pathway, CvME, is a better option to achieve optimal transfection.

2.4 Nuclear entry of gene

Transfection can only be achieve if the gene transverse the nuclear membrane and integrate into the genome successfully. The double membrane of the nucleus prevent gene from crossing and integrating into the genome [7]. According to Elouahabi et al., DNA can enter the nucleus by two mechanism;

1. Passive DNA entry into the nucleus during the cell division; when the nuclear membrane is temporarily disintegrated, transfection is higher. At or near M phase of cell cycle, transfection is higher than during quiescent cell cycle phase such as G1 or S phase.

2. Active transport of DNA through the nuclear pore [7].

2.5 Instrumentation and principle

2.5.1 Luminescence

Luminescence is the emission of light by a molecule. When light is absorbed, electrons moves to a higher orbital which is not a stable state. In order to come back to the stable ground state, the light absorbing molecules releases energy as light at higher wavelength. The light produced in this process can be regarded as phosphorescence or fluorescence depending on the spin states of the molecules, these are describe by Jablonski diagram shown in Figure 2.7 [33].

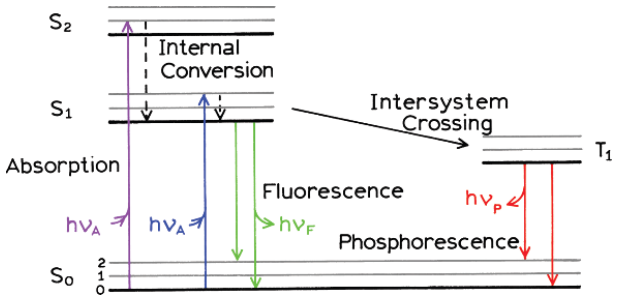

Figure 2.7: Jablonski diagram. When photon emission occurs between states of the same spin (e.g $S_1 \rightarrow S_0$), this is fluorescence. If the spin state of the initial and final energy levels are different (e.g $T_1 \rightarrow S_0$), the emission is called phosphorescence. Two non-radiative deactivation processes in the diagram are; internal conversion and intersystem crossing. Internal conversion is the radiationless transition between energy states of the same spin state. Intersystem crossing is a radiationless transition between different spin states. Adapted from Lakowicz [33].

Immuno-fluorescence

In 1944, Albert Coons demonstrated that antibodies could be fluorescently label. When antibodies are tag with fluorochrome, antibody-antigen complex (Ab-Ag) containing the labelled can be visualised [31]. The labelled bound Ab-Ag complex is visualise with a light microscope equipped with appropriate light sources. There are two methods of labelling molecule immunologically in order to facilitate visualisation. These are;

1. Direct labelling of antibodies ; primary antibodies (pAb) are labelled with a fluorochrome directly by different methods and visualise.
2. Indirect labelling; pAb is unlabelled and its detection depends solely on a labelled secondary antibody (sAb) bound to the pAb [31]. It has several advantages over direct labelling. These are enumerated below:

- It is cheap and flexible. Large range of sAb can be used to detect a pAb.
- Sensitivity is increased by indirect labelling because lot of fluorochrome can be attach [31].

2.5.2 Confocal laser scanning microscopy (CLSM)

Light microscopy can be achieved by two methods; confocal and widefield. The widefield microscopy captures all light emitted by the specimen, and also light outside the focal plane. In contrast, CLSM uses pinhole to remove out of focus light to image thin optical plane. CLSM prevents out of focus blur from being detected. The pinhole is placed between the objective lens and the detector through which only light in focus passes thereby allowing only light from focused object to reach the detector [34].

Principle of CLSM

CLSM uses point illumination and a pinhole in an optically conjugate plane in front of the detector to eliminate out-of-focus signal. Light emission from a laser is directed and focused onto the specimen by scanning mirrors and the laser is scanned line-by-line. Fluorescence emitted from the specimen passes back through the objective to a dichromatic mirror. A dichromatic mirror reflects light shorter than a certain wavelength, and passes light longer than a particular wavelength to the detector. The light that passes is converted into electrical signal by a photomultiplier tube (PMT). The electrical signal is converted to image which is displayed on the computer monitor. The optical configuration of CLSM is shown in Figure 2.8 [34].

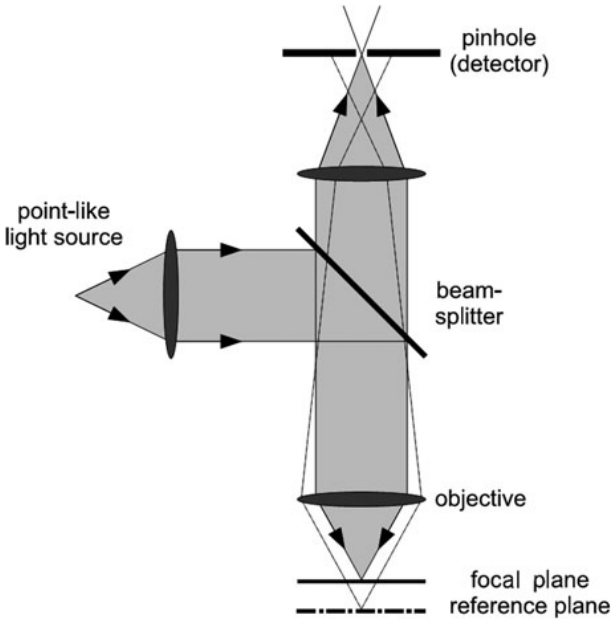

Figure 2.8: The optical configuration of confocal laser scanning microscope (CLSM). It describes the important component responsible for the quality images and it wide range application in research. The light passes through an objective and it is directed to the sample. The light emitted or transmitted by the sample is reflected back and detected. confocal laser scanning microscope pinhole conjugates to the focal plane, so that only light in focus objective can reach the detector. Adapted from Dieing et al. [34].

2.5.3 Differential interference contrast microscopy (DIC)

DIC microscope introduces contrast to specimen [35]. When light passes through a cell via different optical path, contrast is introduced into the sample when this light meets as shown in Figure 2.9. Light beam is separated by a double-refracting cemented prism [35]. It passes through a polarizer that produces a plane polarised light at an angle 45^0. The polarised light is transferred to a wollaston prism (beam splitter) which splits the beam into ordinary and extraordinary ray. The rays passes through the condenser, the specimen

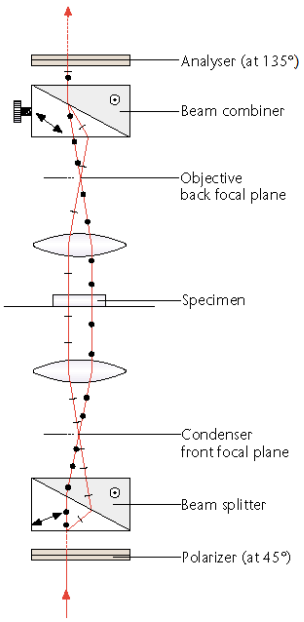

Figure 2.9: The optical configuration of differential interference contrast (DIC) microscope. It describes the important component and it working principle. DIC generates better contrast images. DIC uses additional component to the convectional light microscope to acquire images of better contrast. This include the Polarising filter (45^0), wallaston filter, condenser lens, wallaston prism and polarising filter (135^0). Adapted from Oldfield [35].

and the objective and it is recombined by another wollaston prism. This combined ray is then sent to an analyser set at an angle 135^0. Finally the rays are seen in the eyepiece as a contrast and clear image. The optical configuration of DIC is shown in Figure 2.9 [35].

2.6 Colocalisation

Colocalisation can be define as an overlap in the physical distribution of the molecular populations within a three-dimensional volume. This overlap can be either partial or complete. Colocalisation can be perform simply by image overlaying methods or image analysis [36]. Image analysis methods involve using the statistical approaches such as Pearson's correlation, Mander's coefficient etc [36]. For the purpose of this work, Mander's and Pearson's statistical approaches to quantify colocalisation will be discuss. Combinatory approaches of correlation is recommended as the best. Combinatory approach i.e combination of different colocalisation coefficients will help in comparing of results derived from each coefficient. Comparing the coefficient results help to crosscheck the data gotten by one method with the other method.

2.6.1 Pearson's correlation (PC)

Pearson's correlation describes the extent of overlap between image pairs. PC does some averaging of pixel information and it values ranges from -1 to +1 [36]. Zero connotes no correlation, -1 connotes a negative correlation between the structures, while +1 connotes perfect correlation. PC calculates the distribution from a scattered plots/fluorogram. A fluorogram plots the pixels grey values of two images against each other. In the fluorogram, the intensity of a given pixel are used as the y-coordinate against the intensity of the corresponding pixel, x-coordinate [36]. PC has been recognised to be useful for first estimate of colocalisation. See equation (7.7) in appendix (colocalisation coefficient) for Pearson's coefficient formular.

2.6.2 Mander's coefficient(MC)

Mander's coefficient (MC) is based on PC. It ranges from 0 to 1. Zero connotes non colocalisation while 1 connotes 100% colocalisation between the images being analysed [36]. MC describes the contribution of one channel to the colocalised area so that M_1 and M_2 are the representation of the two channels. The formulas for calculating Mander's coefficient are shown in equations (7.8) and (7.9) in the appendix (colocalisation coefficient).

Where no conclusion can be made with these two colocalisation quantification coefficients, other coefficients such as overlap coefficient according to Mander's, overlap coefficient K_1 and K_2 and colocalisation coefficient m_1 and m_2 can be applied [36]. The mathematical definitions of these coefficients are shown in the appendix (colocalisation coefficients).

Chapter 3

Materials and Methods

3.1 Cell culture

HeLa cells (Human cervical carcinoma cells), a goodwill from Professor Marit Otterlei (Department of cancer research and molecular medicine), NTNU, were cultured in Dulbeco's Modified Eagle's Medium (DMEM) at a passage of 70% confluent, 37^{o}C in 10% CO_2. The DMEM was supplemented with 5% (v/v) fetal bovine serum (FBS) (sigma aldrich, St Louis, MO, USA), 2mM non essential amino acids (sigma aldrich, St Louis, MO, USA), 2mM L-glutamine (sigma aldrich, St Louis, MO, USA). HeLa cells were splitted twice a week. In order to split the cells, DMEM was sucked away followed by washing with 5mL phosphate buffer saline (PBS) (sigma aldrich, St Louis, MO, USA). After removing the PBS, 3mL of trypsin was added to the flask to detach the cells and incubation at 37^{o}C for 3-5mins follows. The effect of trypsin was stopped by adding 10ml DMEM so as to avoid degradation of cellular protein. A droplet of the cell suspension was added to the Brukwald counting chamber while the rest of the cell suspension was centrifuged at 1500rpm for 5 minutes. The supernatant was discarded after the centrifugation, and the cells diluted in DMEM to a proper concentration. For HeLa cells line, a total of 2×10^6 cells were added to the new T_{175} flask which corresponds approximately to a 1:8 splitting of the cells.

3.2 Cell seeding for experiment

HeLa cells cultured in supplemented DMEM media were seeded in 8-well Lab-tek II chamber slide (Nalge Nunc, Naperville, IL, USA) at 1×10^5cells/well 24 hours before the experiment. This allows the cells to attach properly and be metabolically stabilised before the experiment. All reagents which were to be added to cells in larger amount were preheated to 37^{o}C in a water bath (physiological temperature). Inspection of the cells during experiments was carried out with a phase contrast transmission microscope (Leica, DMIL, Buffalo grove, TX, USA.) with objectives of 10x and 20x. This is to monitor the cell

morphological appearance and reactivity to solutions and reagents.

3.3 Chitosan

The two types of Chitosan used as gene carrier in this experiment were LCO and SBTCO, curtailed by Strand et al. [4]. LCO with a number average degree of polymerization (DPn) of 42 was prepared by nitrous acid depolymerisation of completely deacetylated chitosan ($F_A < 0.002$) [3]. SBTCO used was prepared from depolymerised chitosan (DPn = 34) simultaneously branched and substituted with AAM through 2,5-anhydro-D-mannose at the chitosan reducing end. These chitosans were dissolved in 2 mg/ml in milliq water (5-prime, Gaithersburg, MD, USA), sterile filtered and stored in aliquot at -20^oC . They were labelled with Alexa 488 (Invitrogen, Eugene, OR, USA) using a molar ratio of 1 dye molecule per 200 glucose residues.

3.4 Plasmid DNA

A reporter plasmid (gWiz Luc) (Aldevron, Fargo, ND, USA) with a cytomegalovirus promoter and the firefly luciferase (Luc) genes, approximately 6.7 kbp long was used. A stock solution of plasmid DNA was diluted to a concentration of 0.5 mg/ml in sterile milliq grade water. The DNA was labelled with a fluorescence dye before being used for polyplexes formation.

1. TOTO-3 Iodide; TOTO-3 iodide (Invitrogen, Eugene, OR, USA), an intercalating cyanine dye was used to label DNA at the start of this work. The concentration of TOTO-3 was 0.25mg/ml giving a stoichiometry mix of 1 label per 50bp DNA. TOTO-3 was excited with laser line 633nm helium neon (HeNe).

2. Cy5 Dye; Cy5 is a cyanine fluorescence dye that covalently binds DNA. The concentration of Cy5 was used according to Mirus (Mirus, Madison, WI, USA), giving a stoichiometry mix of 1 dye molecule per 50bp DNA. The labelling was done at room temperature in the dark 24 hours before use.

3.5 Polyplexe formation

Chitosan-DNA polyplexes was prepared by the self-assembly method, by adding chitosan to DNA in sterile milliq water. This was done during intense stirring on a vortex machine (Heigar laboratories Oslo, Norway). The polyplexes were prepared with a constant DNA concentration of 13.3μg/ml, A/P ratio 5:1. The polyplexes were incubated for 30 minutes at room temperature before being added to the cells. Prior to incubation of cells with polyplexes, the polyplexes formed were diluted at a ratio of 1:2 with optiMEM (Gibco)

(Invitrogen, Eugene, OR, USA) that was supplemented with 270 mM mannitol (sigma aldrich, St Louis, MO, USA) and 20 mM HEPES (Gibco) (Invitrogen, Eugene, OR, USA) to adjust the osmolarity to 300 mOsm/kg and pH to 7.2. The same procedure was applied to both LCO and SBTCO polyplexes.

3.6 Caveolar vesicle function

Cholera toxin subunit B (CTB) is known to trigger the pinching off of caveolar vesicle, hence it was used to test functional caveolar. HeLa cells were washed with 300μl Hank's buffer salt solution (HBSS) (Invitrogen, Eugene, OR, USA) and incubated with 0.1$\mu g/ml$ Alexa 488 fluorescent label CTB (Invitrogen, Eugene, OR, USA) for 2 hours. The CTB was removed and the cells were incubated in DMEM for 1 hour and 3 hours. Incubated cells were extensively washed and fixed with 4% paraformaldehyde. After fixation, the cells cav containing structures were immunostained and the slides were imaged using CLSM.

3.7 Cell incubation with double labelled polyplexes

HeLa cells seeded in the 8 chamber Lab-tek II chamber slide were washed in 300μl HBSS and incubated with 150μl polyplexes. The incubation was carried out for 15 minutes, 1 hour and 3 hours. The same procedure was applied to both LCO and SBTCO polyplexes.

3.8 Cell Fixation and permeabilisation

HeLa cells were fixed by addition of 150μl 4% paraformaldehyde for 15 minutes. This is quick-washed with 500μl PBS and another washing step with 500μl PBS for 5 minutes. Cells were permeabilised after fixation with 300μl 0.5% (v/v) triton X100 (sigma aldrich, St Louis, MO, USA) for 10 minutes. This was followed by three times washing steps with 500μl PBS. The duration of each of these washing steps is 5 minutes.

3.9 Caveolin staining

Cav were stained using indirect immunostaining technique. Before the immunostaining, potential binding site for sAb which can stimulate non specific binding were blocked with 300μl blocking buffer (5% goat serum (Vector laboratories, Burlingame, CA, USA)) and 0.3% triton-X100 for 60 minutes in room temperature. After blocking, pAb, polyclonal rabbit anti phospho caveolin-1 (PTYR14) (sigma aldrich, St Louis, MO, USA), 5$\mu g/ml$, diluted from stock solution 1.0mg/ml was added. Cells were incubated with 100μl pAb for 60 minutes in a humidifying chamber at room temperature. After addition of pAb, three

washing steps followed. The first and second washing was carried out in 500μl PBS for 5 minutes while the third washing lasted for 2 hours in 500μl PBS.

After these washing steps, the fixed cells were incubated with Alexa 555 labelled sAb (Alexa555-sAb) (goat anti-rabbit IgG) (Invitrogen, Eugene OR, USA), 5$\mu g/ml$, diluted from stock solution 2.0 mg/ml. Incubation with Alexa555-sAb was carried out for 30 minutes in a humidifying chamber. Alexa555-sAb was micro-centrifuged for 5 minutes at 3400rpm before application so as to extract supernatant free of aggregates. After the incubation, the cells were washed in 3 steps as describe for the pAb above. To detect autofluorescence, cells were incubated with antibody buffer (7.0% albumin bovine serum (ABS) (Sigma aldrich, Norway), 0.3% triton-X100 (v/v)) only and washed in three steps as describe earlier. After the washing, HeLa cells were mounted with a drop of prolong gold antifade reagent(Invitrogen, Eugene, OR, USA) and covered with a cover glass, number 1.5 (0.16-0.19mm thickness), 24 $\times$ 50mm size (Corning, Corning, NY, USA).

3.10 Confocal Laser Scanning Microscopy

In all cases, except otherwise stated, HeLa cells seeded and fixed were examined using an LSM 510 (Carl Zeiss Jena GmbH, Germany), equipped with an alpha plan-fluar 100x/1.45 oil objective or C-apochromat$\times$ 40x/1,2 W corr objective. Cy5 DNA labelled was excited with 633nm HeNe laser line while the Alexa 488 labelled chitosans were excited using a 488nm argon laser line respectively. The filters used for detecting the emission were BP651nm-704nm (HeNe) and BP500nm-550nm (argon laser). The Alexa555-sAb was excited with 543nm HeNe laser and the filter used for detecting the emission was BP565-615IR.

Images (616 $\times$ 616 pixels) were recorded in Z stacks. The dwell time of the laser power was 1.26$\mu secs$ and the scan zoom 2. Stacks consisted of 70-80 slides and pinhole diameter used were 164μm (543nm excitation), 148μm (488nm excitation) and 192μm (633nm excitation). Settings used were chosen so as to utilise the whole dynamic range thereby avoiding saturation and low intensity.

To test linear unmixing, the caveosomes were imaged in lambda mode. The meta-channel of the Zeiss LSM 510 was used to acquire the lambda series, and emission was recorded in the range 548 to 623 nm, in steps of 10.70 nm. Reference samples of single-labelled specimens (Alexa 488-labelled chitosan and Alexa 555-labelled caveosomes) were imaged under conditions identical to those used when imaging the caveosomes in the multilabelled specimen, and the reference spectra for the two Alexa dyes were acquired and stored in the spectra database for linear unmixing purposes. The chitosan and the DNA was imaged as described earlier.

3.11 Image processing

Images were restored by deconvolution using amira 5.3.1 software (Amira, San Diego, CA, USA). The point spread functions (PSF) were generated by imaging fluorescence beads (PS-speck microscope point source kit (P7220) (invitrogen, Eugene, OR, USA)) of diameter $0.175 \pm 0.005 \mu m$ with CLSM. Beads of different colours were mounted on separate slide in prolong gold antifade reagent. The green, orange and red beads were imaged with settings identical to those used for imaging chitosan, caveosomes and DNA, respectively. Individual beads from each stacks were picked in the amira software and an average bead was computed, corresponding to the PSF. Combining the Z stacks images of cells and corresponding PSF and performing the deconvolution gave a stack of images devoid of out of focus blur. The deconvolution was performed as recommended in the amira user's guide (border width or guard band region used was 8 pixels for x, y and z and the number of iteration is 20).

3.12 Image Analysis

Quantitatively, CLSM images were analysed in the imageJ software (Mac bio-photonics, Hamilton, ON, Canada), based on the region of fluorescence. The number of thresholded pixels and the fluorescence intensity in those pixels were quantified. Intracellular DNA and caveosomes were counted. Each Z stacks image was splitted into three separate stacks or channels. The corresponding DIC image was studied and region of interest (ROI) which delineated the cells was drawn. The ROI was copied to each of the three stacks, and fluorescence confined by the ROI was analysed with respect to the number of thresholded structures, the mean volume and the total volume, using the plugin object counter 3D. The mean volume of DNA describes the average of all volume of intracellular DNA either bound or dissociated from the chitosan while the total volume sum the volume of the entire DNA in the cell. The mean volume of caveosomes describes the average volume of caveosomes in the cell and the total volume sum up all the caveosomes volume in the cell. Also, quantification of colocalisation was carried out using the plugin intensity correlation analysis.

3.13 Data Analysis

Excel 2007 (Microsoft, Redmond, WA, USA) was used for subsequent calculation of the mean, standard deviation (SD), t-test and chart plotting. Unless otherwise indicated, all of the measured data were collected and expressed as mean values ± SD. The statistical differences between the mean values were investigated using ANOVA in conjunction with two-sample, one-tailed students t-test assuming non-equal variances. The differences between the means were considered significant at $p < 0.05$.

Chapter 4

Results

4.1 Optimisation of caveolin staining

The visualisation of cellular structures based on fluorescence requires an optimal staining of the structures. Cav were indirectly stained using pAb and Alexa555-sAb. In order to achieve an optimal staining for cav, concentrations of the pAb and Alexa555-sAb were tested. Different concentration of pAb and Alexa 555-sAb were combined to see which gives the best image with maximal fluorescence intensity and minimal non-specific binding of antibodies. The optimal concentration combination was chosen based on qualitative analysis of the images acquired by CLSM. Figure 4.1 summaries the results of antibody combinations. These images qualitatively show the results of the tested antibodies concentration. First, cells were fixed and stained for cav without incubating with something that triggers endocytosis. The CLSM images showed that the cav structures were located in the cell membrane which were seen as fine green dots in Figure 4.1A.

Next, cells were incubated with CTB prior to cell fixation and staining. Preincubation of HeLa cells with $0.1\mu g/ml$ CTB for 2 hours triggers the release of cav containing structures from the membrane domain into the cytoplasm (Figure 4.1B). After incubating cells with CTB, fine dots seen in plasma membrane (Figure 4.1A) were now observed in the cell cytoplasm with little or no fluorescence in the membrane.

With the green dots being localised in the cell cytoplasmic region after incubation with CTB, images acquired using different antibodies combination were compared. This comparison was done to choose the optimal pAb and Alexa 555-sAb combination. The combination of $5\mu g/ml$ pAb to $5\mu g/ml$ Alexa 555-sAb gave best result (Figure 4.1B and C). Other combination of pAb and Alexa 555-sAb either resulted in too much non-specific binding of the antibodies or low fluorescence signal from the label.

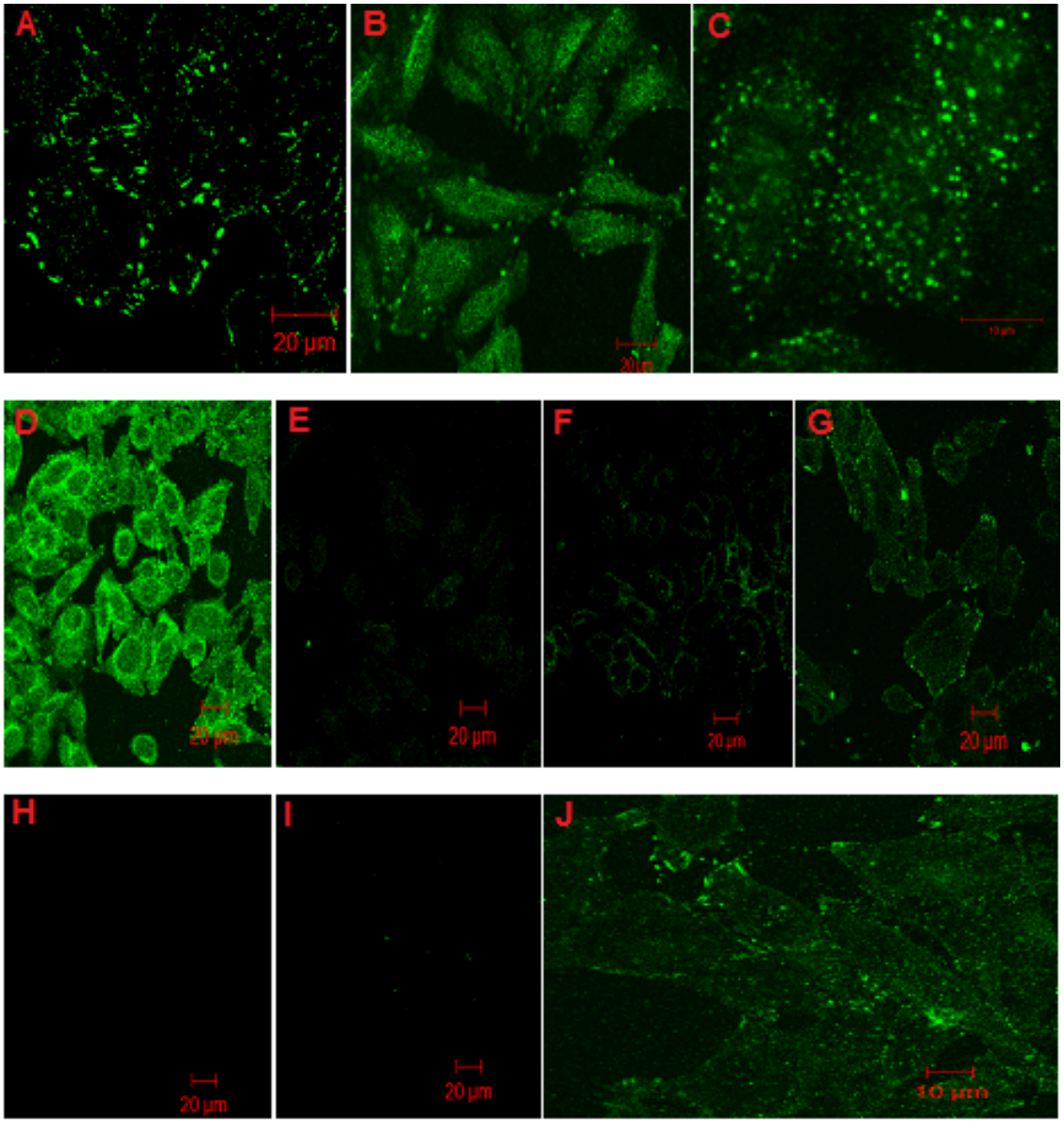

Figure 4.1: Optimisation of cav staining. Optimal staining of cav was achieved by varying the concentration of pAb and Alexa 555-sAb. Cav (green), CTB (red). A: No incubation with CTB, $5\mu g/\mu l$ pAb and $5\mu g/ml$ Alexa 555-sAb. B: $5\mu g/ml$ pAb and $5\mu g/ml$ Alexa 555-sAb. C: $5\mu g/ml$ pAb and $5\mu g/ml$ Alexa 555-sAb in scan zoom 2. D: $50\mu g/ml$ pAb and $5\mu g/ml$ Alexa 555-sAb. E: $5\mu g/ml$ pAb and $2.5\mu g/ml$ Alexa 555-sAb. F: $10\mu g/ml$ pAb and $1\mu g/ml$ Alexa 555-sAb. G :$10\mu g/ml$ pAb and $5\mu g/ml$ Alexa 555-sAb. H: $0\mu g/ml$ pAb and $1\mu g/ml$ Alexa 555-sAb. I: $0\mu g/ml$ pAb and $5\mu g/ml$ Alexa 555-sAb. J: $5\mu g/\mu l$ pAb and $5\mu g/ml$ Alexa 555-sAb with mild washing. In all images except A, HeLa cells were incubated with 0.1 $\mu g/ml$ CTB, fixed in 4% paraformaldehyde and immunostained for caveolin. All images were acquired using scan zoom 1 except C and J (scan zoom 2)

Non specific binding of antibody was observed when $50\mu g/ml$ pAb was labelled with $5\mu g/ml$ Alexa 555-sAb (Figure 4.1D). Combination of $5\mu g/\mu l$ pAb with $2.5\mu g/\mu l$ Alexa 555-sAb, $10\mu g/\mu l$ pAb with $1\mu g/\mu l$ Alexa 555-sAb and $10\mu g/\mu l$ pAb with $5\mu g/\mu l$ Alexa 555-sAb resulted in low fluorescence signal as a result of low sAb binding the pAb (Figure 4.1E-G). Two controls were always included; the first tested for non specific binding of Alexa 555-sAb in the absence of pAb while the second control tested for autofluorescence. For the first control, the concentration of the Alexa 555-sAb was varied between $5\mu g/\mu l$ and $1\mu g/\mu l$ which gave no signal (Figure 4.1H). In the other control slide, no autofluorescence was observed (Figure 4.1I).

In the process of optimisation, the duration for the washing steps was also varied in order to remove excess antibodies and reduce non-specific binding of the antibodies. At the start, fixed cells were washed in PBS three times for 5 minutes after each incubation with antibody. Images acquired with this mild washing were usually cloudy with non-specific binding of antibodies (Figure 4.1J).

The duration and parameters for washing were adjusted in order to remove this non-specific binding. Extensive washing step which was a long duration washing on a shaker carried out twice (5 minutes each time), and a third time for 2 hours was later applied. This washing was applied after incubation with pAb and with Alexa 555-sAb. Application of this extensive washing resulted in good, clear and less noise images. It is worth noting that, in all cells incubated with CTB, the CTB was located in the cells where it colocalised with the green dots (image overlay) as shown in Figure 4.2. Figure 4.3 shows a 3D image

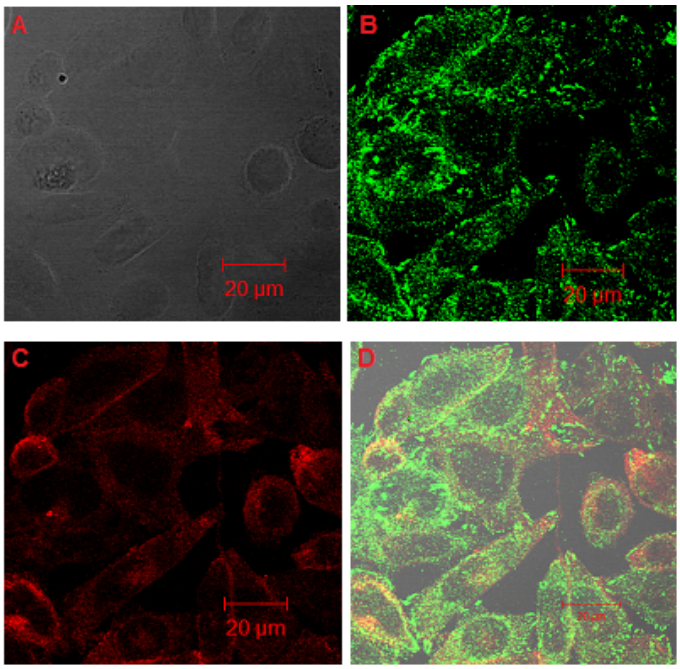

Figure 4.2: CTB colocalised with the green dots of cav protein. DIC image (A), Caveosome (B), CTB (C) and combine image (D). Cells were incubated in $0.1\mu g/ml$ CTB and fixed in 4% paraformaldehyde, immunostained for cav and imaged with CLSM.

of an optimised caveosomes staining.

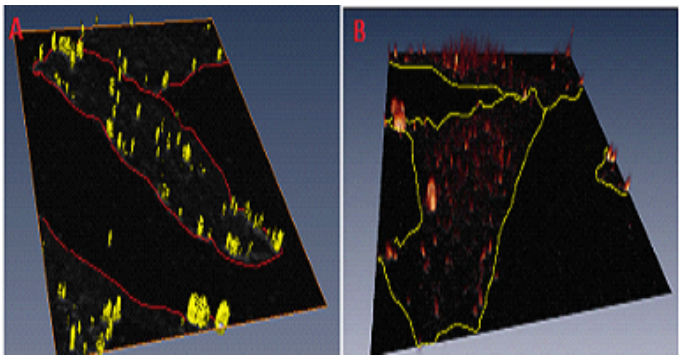

Figure 4.3: Three dimensional images of caveosomes. 3D image of caveosomes after optimal staining procedure. The caveosomes were represented in yellow (A) and red (B). The highlighted area marks the border of cells (cell membrane). The caveosomes were located and randomly distributed in the cell cytoplasm. A and B were created with different visualisation technique in amira software.

4.2 Polyplexe Staining

DNA had to be labelled with a fluorescence dye producing minimal crosstalk with Alexa fluor 488 which was attached to chitosan, and Alexa fluor 555 used for cav immunostaining. First, TOTO-3 iodide, an intercalating dye was chosen as a label for the DNA. Cy5, a covalent binder of DNA would have been better option, but because it induces aggregates it was not the first choice for DNA staining. After subsequent experiment with TOTO-3 dye, it was observed that the dye smeared out within the cell as shown in Figure 4.4 (page 27). The smearing was observed after cells were extensively washed in PBS. The signal of the DNA expected to be dots appears as a cloudy background as seen in Figure 4.4B and D.

To verify the smearing, cells were imaged after fixation and each washing step and the washing was monitored by CLSM (Figure 4.5) (page 28). Before washing, the polyplexes were in ample amount in the media with some polyplexes bound to the cell surface and the rest located intracellularly (Figure 4.5A-D). After fixation, the TOTO-3 dye had started smearing out (Figure 4.5E-H). After 2 hours and 30 minutes of washing, the TOTO-3 had smeared more and no DNA dot can be seen (Figure 4.5I-L). After the last washing step, the chitosan (green) were still localised as fine dots while the DNA (red) were totally smeared out (Figure 4.5M-P).

Due to smearing by TOTO-3, the fluorophore was replaced with Cy5. The efficacy of the Cy5 dye was seen, as subsequent experiment lacks this smearing out of DNA label (Figure 4.6) (page 29). The DNA nanoparticles were seen as distinct dots which defines their location in the cell. Difference in efficacy of the two dyes in this experiment can be seen by comparing images in Figure 4.6 and Figure 4.7 (page 29).

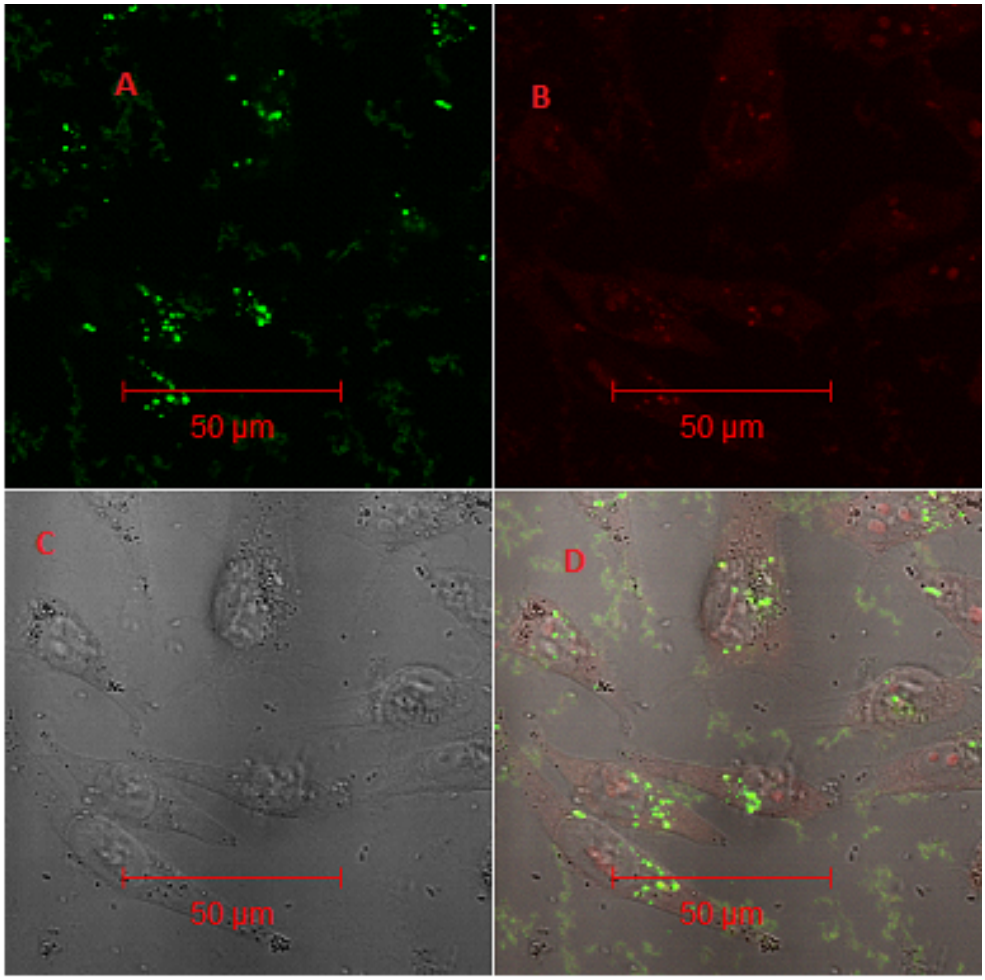

Figure 4.4: TOTO-3 iodide smearing. TOTO-3 iodide was smeared out in the cells when washed extensively. The Alexa 488 labelled chitosan (green) (A), smeared out TOTO-3 labelled DNA (red)(B), DIC image (C) and combined images (D).

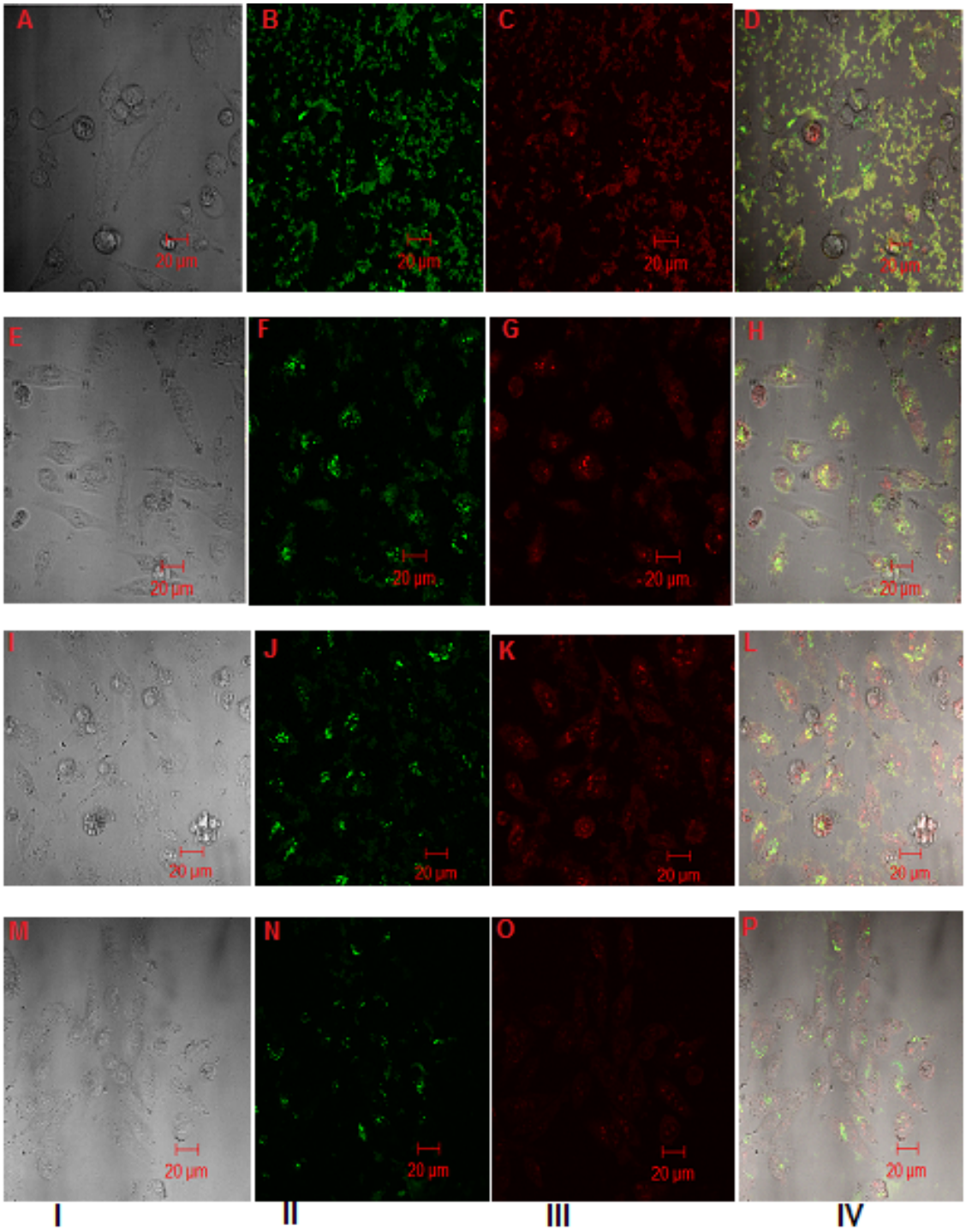

Figure 4.5: The smearing of TOTO-3 iodide in the cells increases as the cells were extensively washed. The images shows the DIC (I), labelled chitosan (green)(II), labelled DNA (red)(III) and the combined image (IV). The cells after 2 hours incubation period of the polyplexes without any washing step (A-D). The cells during the blocking steps after being fixed with 4% paraformaldehyde (E-H). The cells after 2 hours 30 minutes extensive washing in PBS (I-L). The cells after final washing step, total of 6 hours washing in PBS (M-P). Before any washing steps, the DNA appears as red dots (C). The red dots smear out as the cells were being washed to remove non-specific binding of antibodies and polyplexes in the surrounding media.

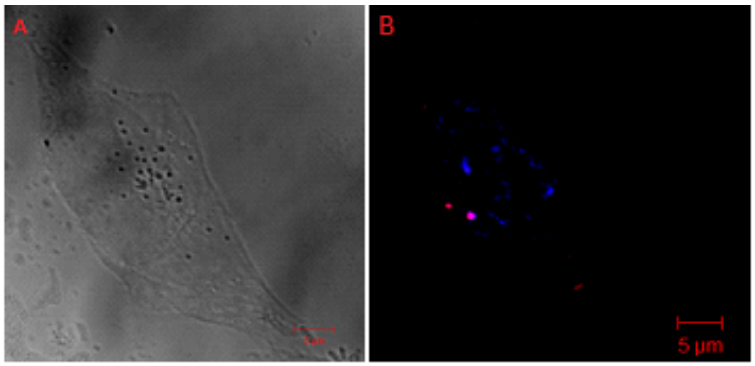

Figure 4.6: Cy5 covalently binds DNA and do not smear out within the cell. DIC image (A) and polyplexes (B). Chitosan (blue) and DNA (red).

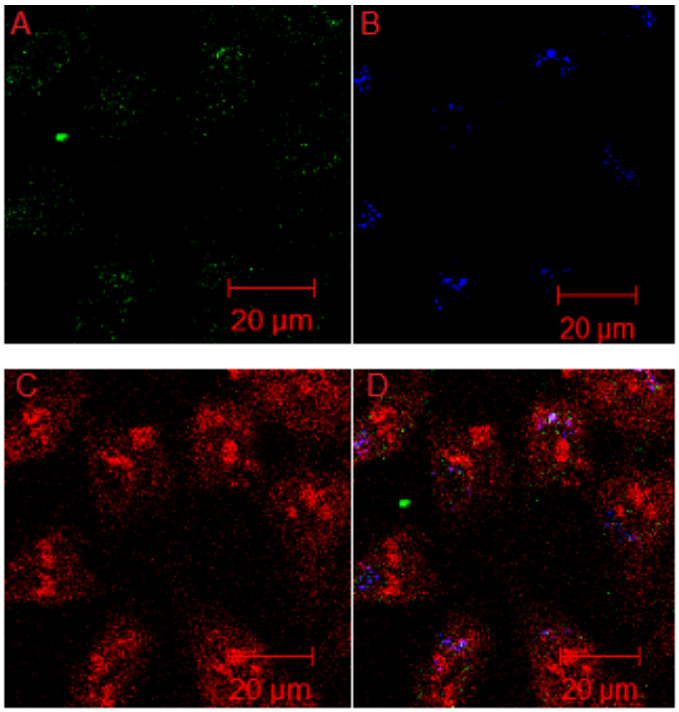

Figure 4.7: Extensive smearing of TOTO-3 iodide after washing steps in PBS. caveosomes (green)(A), Chitosan (blue)(B), DNA (red)(C) and combine images (D).

4.3 Comparison based on intracellular DNA and caveosomes

Analysis of intracellular DNA and caveosome will give more insight into the intracellular processing of these polyplexes. Comparison based on these features were more related to the CvME since caveosome is of paramount importance in this analysis. The intracellular DNA and caveosome were analysed qualitatively and quantitatively. This helps to compare and to establish what was observed in the experiment which describes the polyplexes intracellular fate.

4.3.1 Qualitative analysis of intracellular DNA in HeLa cells

The intracellular DNA content transported by the polyplexes was examined qualitatively by comparing CLSM images from cells incubated with these polyplexes (Figure 4.8 - Figure 4.13).

At 15 minutes incubation period, little DNA were observed in HeLa cells incubated with either SBTCO polyplexes (Figure 4.8) or LCO polyplexes (Figure 4.9).

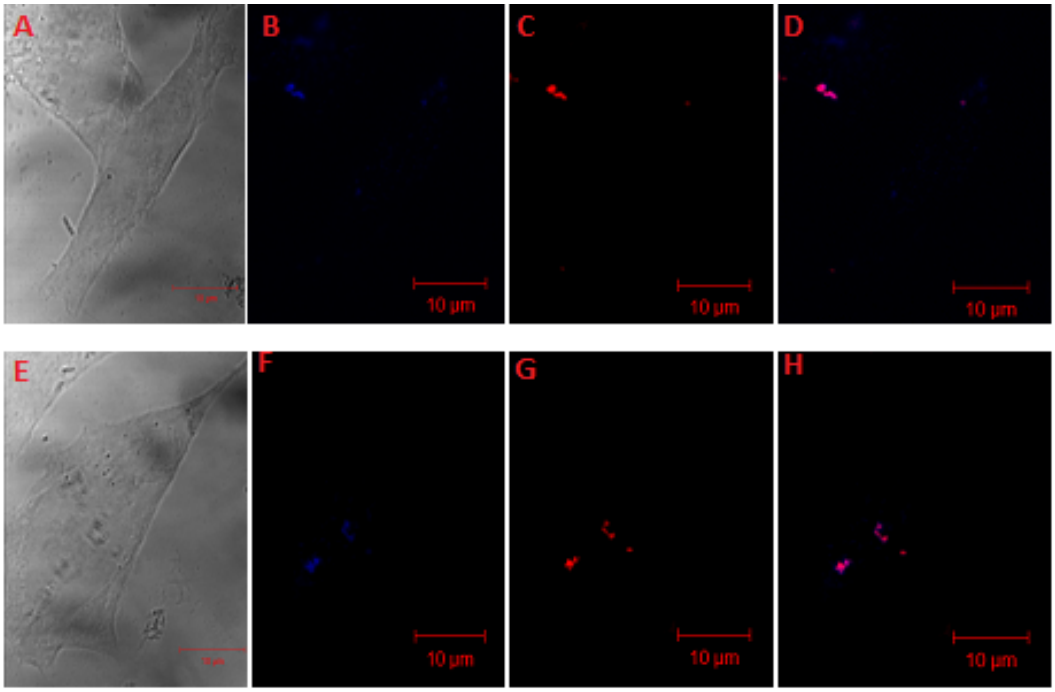

Figure 4.8: Intracellular DNA at 15 minutes period of incubation with SBTCO polyplexes. DIC images (A and E), SBTCO (blue)(B and F), DNA (red) (C and G) and combined images (D and H). At 15 minutes incubation period, little DNA can be seen in the cells. Although the DNA content were low, the chitosan was higher.

Although images from these cells show little DNA dots, SBTCO polyplexes incubated cells

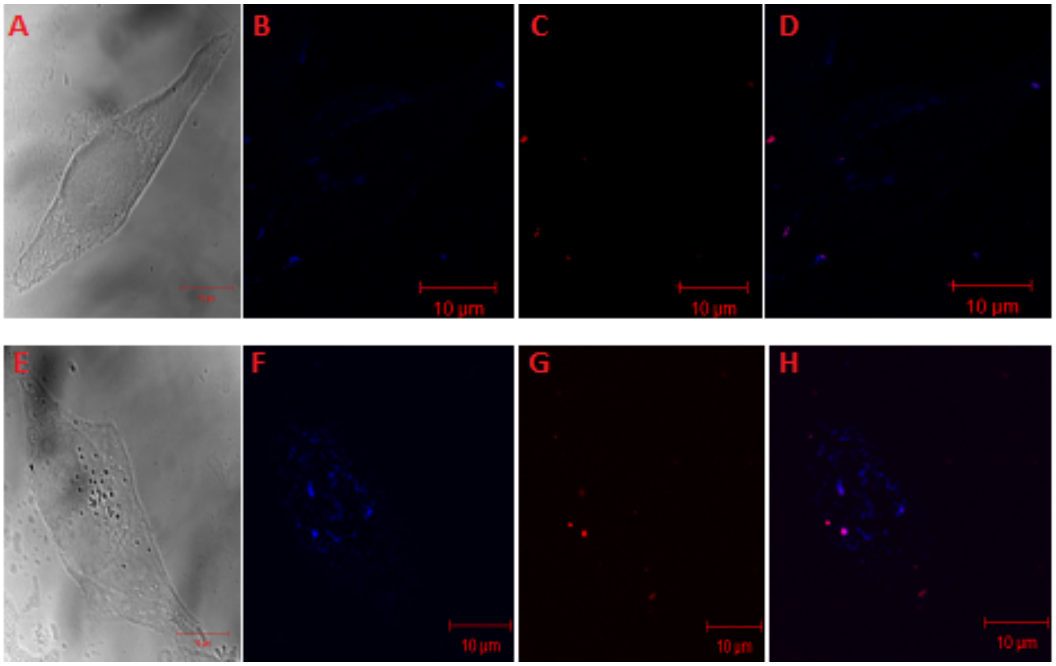

Figure 4.9: Intracellular DNA at 15 minutes period of incubation with LCO polyplexes. DIC images (A and E), LCO (blue)(B and F), DNA (red) (C and G) and combine images (D and H). At 15 minutes incubation period, few DNA dots were observed.

had a higher number of DNA dots (Figure 4.8) than LCO polyplexes (Figure 4.9) at the same 15 minutes period of incubation.

At 15 minutes of incubation, though little DNA were localised intracellularly, chitosan content exceeds the DNA content in all cells because of excess chitosan used in complexation (A/P ratio = 5). The chitosans were dispersed in the cell as distinct dots (blue) while some colocalised with the DNA.

At 1 hour of incubation with the polyplexes, more DNA dots were present inside the cells incubated with SBTCO (Figure 4.10) polyplexes than LCO polyplexes (Figure 4.11). This means the higher DNA content in SBTCO polyplexes incubated cells (Figure 4.10) over LCO polyplexes incubated cells (Figure 4.11) was maintain.

Intracellular DNA in SBTCO polyplexes cells continue to increase at 3 hours incubation time (Figure 4.12). Although the intracellular DNA content also increase in LCO polyplexes incubated at 3 hours (Figure 4.13), lower number of DNA dots were observed in LCO polyplexes incubated cells compared to SBTCO polyplexes incubated cells. Its worth noting that intracellular chitosan increased with time of incubation, and were more than intracellular DNA at all time of incubation.

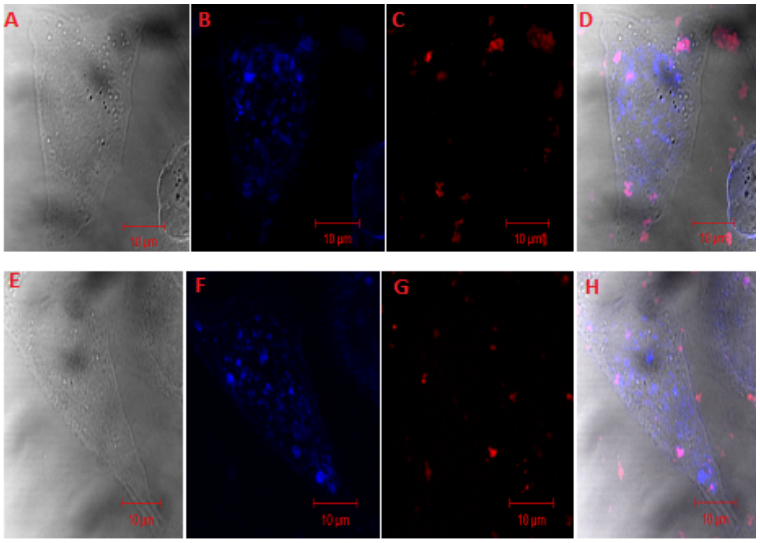

Figure 4.10: Intracellular DNA increased at 1 hour period of incubation with SBTCO polyplexes. DIC images (A and E), SBTCO (blue) (B and F), DNA (red) (C and G) and combined images (D and H) of colocalised polyplexes (purple). Intracellular DNA number increased at 1 hour incubation period of HeLa cells with SBTCO polyplexes. By this time of incubation, the polyplexes spread in the cell cytoplasm. Also, intracellular chitosan content has increased.

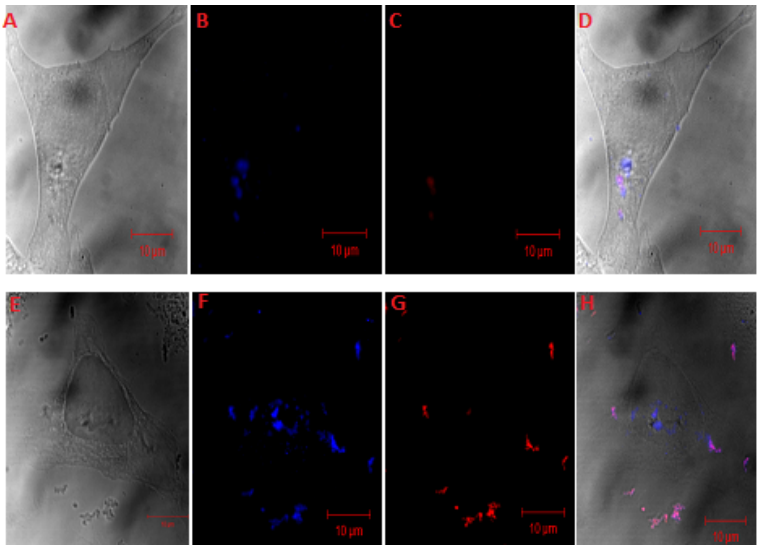

Figure 4.11: Intracellular DNA at 1 hour incubation with LCO polyplexes. DIC images (A and E), LCO (blue) (B and F), DNA (red) (C and G) and combine images (D and H) of colocalised polyplexes (purple). At 1 hour incubation period, the intracellular polyplexes increased.

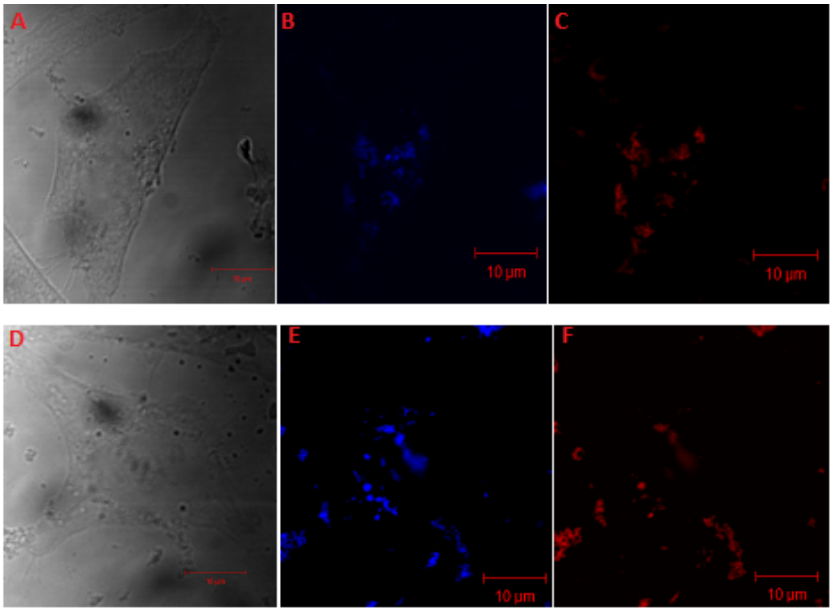

Figure 4.12: Intracellular DNA at 3 hours incubation period with SBTCO polyplexes. DIC images (A and E), SBTCO (blue) (B and F), DNA (red) (C and G) and combine images (D and H) of colocalised polyplexes (purple). At 3 hours incubation period the DNA content were increasing. Also, the chitosan content had increased.

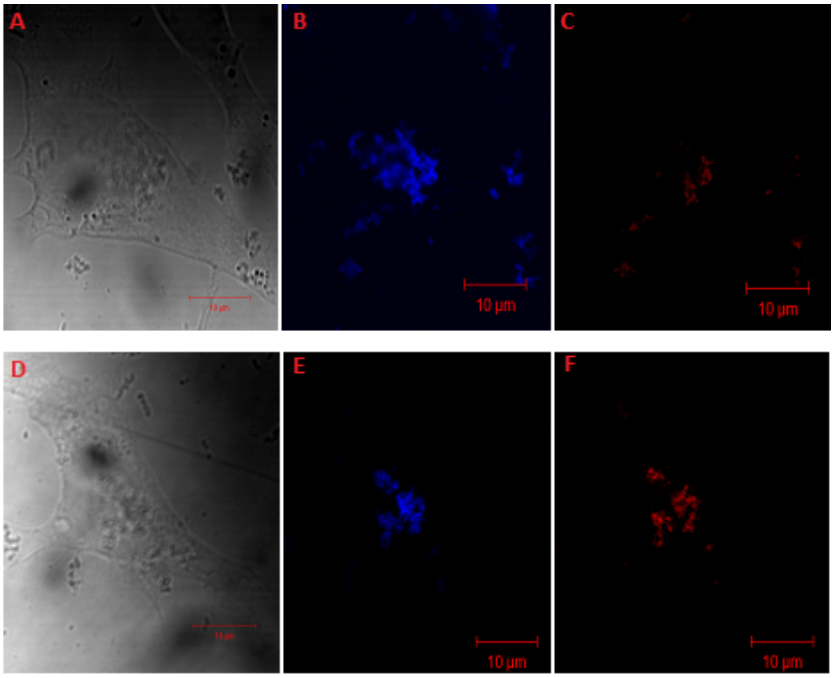

Figure 4.13: Intracellular DNA at 3 hours incubation with LCO polyplexes. DIC images (A and E), LCO (blue) (B and F), DNA (red) (C and G) and combine images (D and H) of colocalised polyplexes (purple). The amount of intracellular nanoparticle had increased. Also, intracellular chitosan had increased.

4.3.2 Quantitative analysis of intracellular DNA content in HeLa cells

In order to verify the images analysed qualitatively, intracellular DNA in HeLa cells incubated with the two types of polyplexes were quantified. Figure 4.14A shows the DNA nanoparticle count per cell. At all incubation time, the number of DNA particles (com-

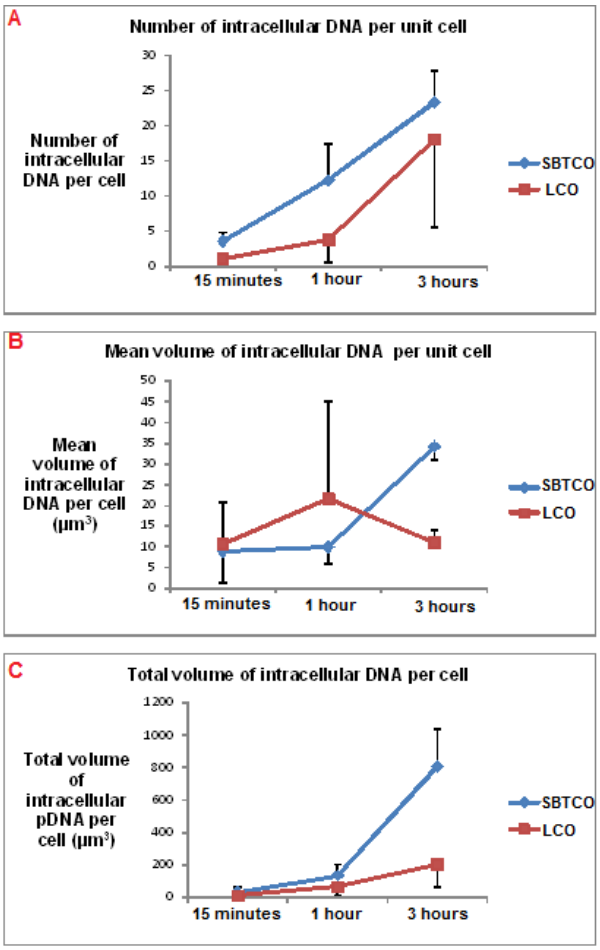

Figure 4.14: Graphical representation of intracellular DNA number, mean volume and total volume per unit cell at different time of incubation with polyplexes. Number of DNA particles per cell (A), mean volume DNA per cell (B) and total volume of DNA per cell (C). Analysis was carried out on Z stack images of (70-80) slides from 5-6 cells.

plexes or dissociated form) in cells incubated with SBTCO polyplexes increased and are higher than those in LCO polyplexes incubated cells. The values for DNA in SBTCO incubated cells were 3.5 ± 1.3 (15 minutes), 12.2 ± 5.2 (1 hour) and 23.3 ± 4.5 (3 hours) which was higher than DNA number in LCO polyplexes incubated cells 1.0 ± 03 (15 minutes), 3.8 ± 3.2 (1 hour) and 18.0 ± 12.5 (3 hours).

At 15 minutes and 1 hour incubation periods, the difference in intracellular DNA number between cells incubated with LCO polyplexes and SBTCO polyplexes were significantly

different ($p < 0.05$). At 3 hours incubation time, though the intracellular DNA in SBTCO polyplexes incubated cells were higher than their LCO polyplexes incubated counter part, the difference was insignificant ($p < 0.05$). This statistical insignificance was due to large SD at 3 hours incubation period.

Mean volume of the intracellular DNA (Figure 4.14B), shows that the mean size of DNA either in polyplexes or dissociated form in SBTCO polyplexes incubated cells increases with time. It reached a value of 34.3 ± 3.3 at 3 hours incubation period. In contrast, the mean volume of DNA in LCO polyplexes incubated cells shows an increase between 15 minutes incubation period (10.6 ± 10.2) and 1 hour (21.6 ± 23.4). At 3 hours of incubation, DNA mean volume in LCO polyplexes incubated cell decreased to 10.8 ± 3.1.

At 15 minutes and 1 hour incubation time, the mean volume of intracellular DNA between the cells incubated with LCO polyplexes and SBTCO polyplexes were insignificantly different ($p < 0.05$). At 3 hours incubation time, the increase in mean volume of DNA in SBTCO polyplexes incubated cells over LCO polyplexes incubated cells was significant ($p < 0.05$).

Figure 4.14C shows that the total volume (i.e. number of DNA particles $\times$ mean volume) of DNA transported by SBTCO polyplexes increases with increasing incubation time. Total volume of DNA, delivered by LCO polyplexes also increases but at a lower rate compare to SBTCO polyplexes transported DNA. At 15 minutes and 1 hour incubation period, the difference in the total volume of intracellular DNA were insignificant between the two polyplexes ($p < 0.05$). At 3 hours incubation period, DNA total volume in SBTCO polyplexes incubated cells increased and reached a value of 809.4 ± 227.23 compare to 202.4 ± 139.3 in LCO polyplexes incubated cells ($p < 0.05$). In summary, quantitative counting confirmed that intracellular DNA transported by SBTCO polyplexes were higher in number, mean volume, and total volume per cell over their LCO polyplexes counterpart especially at 3 hours incubation period.

4.3.3 Qualitative image analysis of caveosomes after HeLa cells were incubated with polyplexes

Analysis of caveosomes in cells incubated with polyplexes were carried out both qualitatively and quantitatively. The qualitative analysis was carried out to show if there were any difference in caveosome dots observed between LCO and SBTCO polyplexes incubated cells. Images of cells incubated with the polyplexes were compared as shown in Figure 4.15. The caveosomes number appears to be of same amount at 15 minutes and 1 hour incubation period as almost the same amount of green caveosome dots concentrated in the cell cytoplasm were observed (Figure 4.15A, B, D and E). In cells incubated for 3 hours, caveosomes were seen to be more concentrated in SBTCO polyplexes incubated cells (Figure 4.15C) than in LCO polyplexes incubated cells.

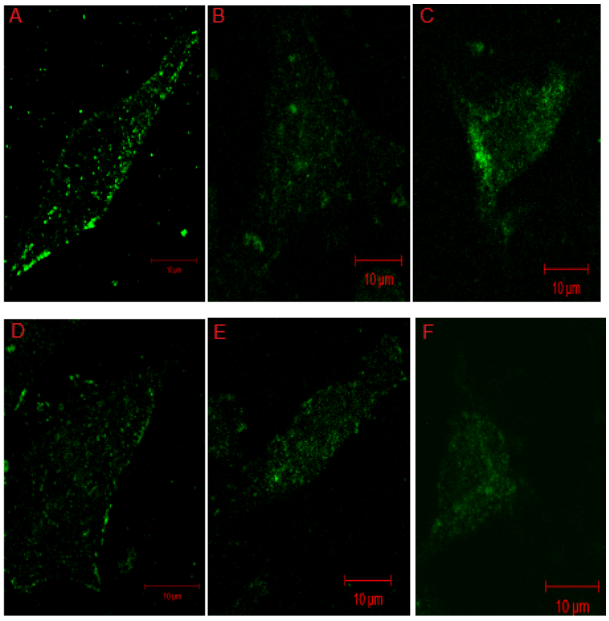

Figure 4.15: Images comparing caveosomes between LCO and SBTCO polyplexes incubated HeLa cells. Cells incubated with SBTCO polyplexes for 15 minutes , 1 hour and 3 hours (A-C). Cells incubated with LCO polyplexes for 15 minutes, 1 hour and 3 hours (D-F). The fluorescence intensity in B,C,E and F look darker because the images were recorded at lower gain (705) to avoid saturation. A and D were acquired at much higher gain (785). The only visible difference in caveosomes were at 3 hours incubation period. At 3 hours incubation, the amount of caveosomes in SBTCO polyplexes incubated cell were higher compared to cells incubated with LCO polyplexes.

4.3.4 Quantitative analysis of intracellular caveosomes after HeLa cells were incubated with polyplexes

Quantitative analysis of the caveosomes number confirmed the images analysed qualitatively. Caveosome number triggered by SBTCO polyplexes increased with time of incubation with highest count at 3 hours incubation time ($p < 0.05$) (Figure 4.16A). The caveosome number in SBTCO polyplexes incubated cells increased moderately between 15 minutes (36.2 ± 34.4) and 1 hour (99.7 ± 96.9) period of incubation. At 3 hours incubation period, caveosome number was 2 times higher than 1 hour count. In contrast, caveosome number in LCO polyplexes incubated cells decreased with time of incubation. LCO polyplexes had highest caveosome number (57.8 ± 44.8) at 15 minutes incubation period which decreased with time. At 3 hours incubation time, caveosome level in LCO polyplexes incubated cells was reduced by 23% (from 52.7 ± 52.0 (1 hour) to 40.8 ± 16.3 (3 hours)). Comparing the caveosome number in SBTCO and LCO polyplexes incubated cell, SBTCO polyplexes incubated cells have higher number of caveosomes at 3 hours incubation period than LCO polyplexes incubated cells ($p < 0.05$).

Figure 4.16B describes the mean volume (average volume of caveosome per cell) of the caveosome per cell in LCO and SBTCO polyplexes incubated cells. At 15 minutes incubation period, both SBTCO and LCO polyplexes incubated cells have approximately

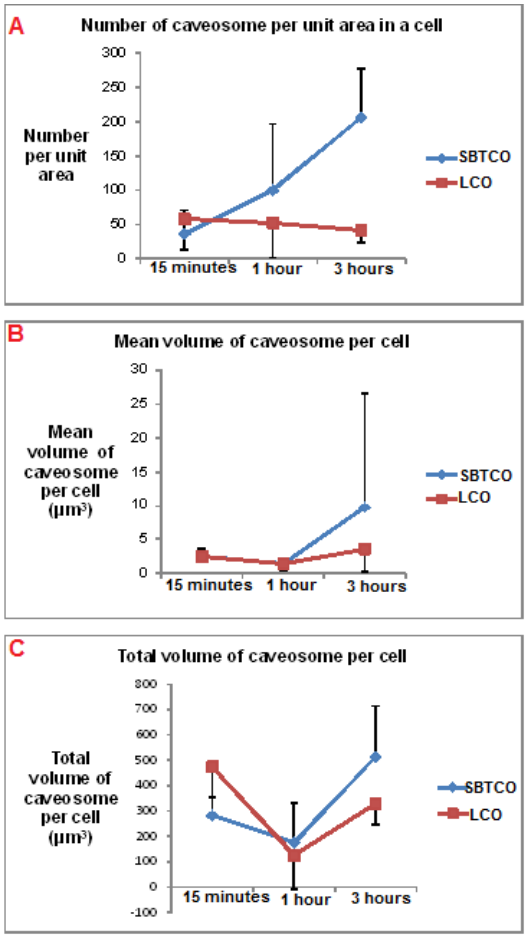

Figure 4.16: Graphical representation comparing caveosomes in cells incubated with SBTCO polyplexes and LCO polyplexes. Number of caveosomes per unit area (average number of caveosome in $1\mu m^2$.) (A), Mean volume of caveosomes per cell (B) and Total volume of caveosomes per cell (C). Analysis was carried out on Z stack images of (70-80) slides from 5-6 cells.

equal mean volume (SBTCO (2.4 ± 1.2) and LCO polyplexes (2.4 ± 0.5)). The equal mean volume was maintained at 1 hour incubation period with a mean volume value of 1.4 ± 0.8 for SBTCO and 1.44 ± 1.06 for LCO polyplexes incubated cells. The equal mean volume changed at 3 hours incubation period with SBTCO polyplexes incubated cells having a higher caveosomes mean volume of 9.7 ± 16.9. At this time, caveosomes mean volume in LCO polyplexes incubate cells increased to 3.5 ± 3.3, i.e., the mean volume of caveosomes in SBTCO polyplexes incubated cells was higher than LCO polyplexes incubated cells at 3 hours. This value is statistically insignificant due to large SD. In summary, the mean volume of caveosome decreased from 15 minutes to 1 hour incubation and peaked up at 3 hours in both LCO and SBTCO polyplexes incubated cells.

Figure 4.16C compares total volume of caveosomes (number of caveosomes $\times$ mean volume of caveosomes) in SBTCO and LCO polyplexes incubated cells. The total volume decreased from 15 minutes to 1 hour incubation time and increased again at 3 hours incubation time

in both polyplexes incubated cells. Although the total volume of caveosome in both LCO and SBTCO polyplexes follow same graph progression (Figure 4.16C), the total volume of caveosomes in SBTCO polyplexes incubated cells was higher than LCO at 3 hours incubation period ($p < 0.05$). The percentage difference in total volume at 3 hours between LCO and SBTCO polyplexes incubated cells was estimated as 36%. In summary, Figure 4.16 shows that cells incubated with SBTCO polyplexes have more caveosomes than cells incubated with LCO polyplexes. The number increased with time and was higher at 3 hours incubation period ($p < 0.05$). Likewise, the mean and total volume of caveosome decreased and later increased at third hour of incubation. At the third hour, caveosomes total volume in SBTCO polyplexes incubated cells were higher than the total volume of caveosomes in LCO polyplexes incubated cells ($p < 0.05$).

4.4 Colocalisation

The colocalisation of molecules within cellular organelles helps to determine the interaction of these structures. Colocalisation of polyplexes with caveosomes will provide information about the location of these polyplexes in relation to caveosome. In order to colocalise polyplexes with caveosomes, Z stacks 3D images of the cell acquired with CLSM were deconvoluted. Deconvolution removed blur from images. Deconvolution of Figure 4.17A resulted into Figure 4.17B. The deconvolution was carried out as described in chapter 3

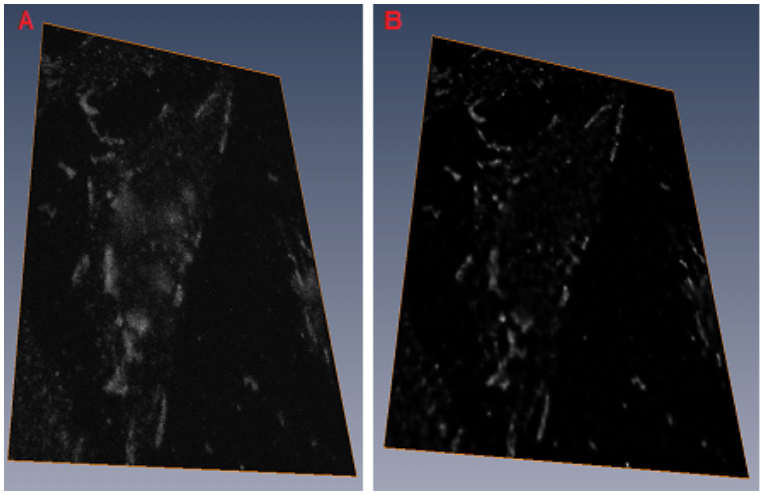

Figure 4.17: Images of caveosomes before and after deconvolution. Deconvolution procedure eliminates blur from microscopic images. Raw image from CLSM (A) and deconvoluted image (B).

with acquisition of beads images using CLSM (Figure 4.18A). These beads were used to generate PSF (Figure 4.18B).

Crosstalk problem can be observed in dual or multicolour experiments. In this experiment, crosstalk made the quantification of colocalisation between polyplexes and caveosomes impossible on raw images from CLSM. Although multitracking or sequential mode was

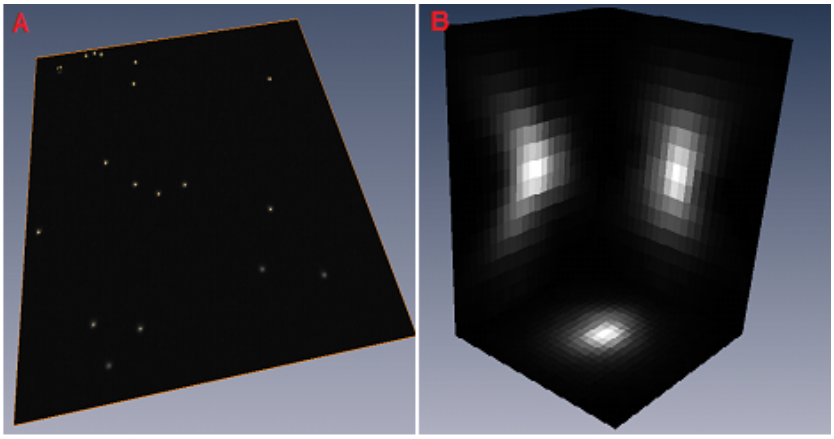

Figure 4.18: Generation of PSF for deconvolution. Image stack of PS-speck microscope point source were acquired with CLSM (A) and converted into PSF (B).

used during imaging, crosstalk was still observed. If the excitation spectra of the dyes do not overlap too much and the concentration of the dyes used are balanced, normally no cross-excitation and bleedthrough is observe in sequential mode. The lasers were turn on and off sequentially to excite one dye per image acquisition. Nevertheless, the laser used to excite the Alexa 555 also excited the Alexa 488 and Cy5 (Figure 4.19). The crosstalk occurred because the excitation spectra of these dyes overlap (Figure 4.20), and the emission from the cross-excited dye was recorded in the wrong channel. If the bandpass filter in front of a detector spans part of the emission spectrum of a cross-excited dye, its emission will be detected together with the emission from the dye that is intentionally excited. The emission spectra of the dyes, for the conditions used in this experiment, are shown in Figure 4.21.

Crosstalk experiments on slides of single labelled polyplexes (no cells) were performed (Figure 4.22 and Figure 4.23). The cross-excitation of Alexa 488 labelled chitosan and Cy5-labelled DNA by the 543nm HeNe laser was confirmed. The degree of colocalisation observed was dependent on the laser power and the detector gain of the caveosome channel. The higher the laser power or gain, the more crosstalk from chitosan and DNA in the caveosomes channel. This was observed as polyplexes lumps identical to those in the chitosan and DNA channel. This cross excitation is illustrated by the changes in the intensity profiles in Figure 4.22 and Figure 4.23. The cross excitation of the Alexa 488 was more pronounced than the cross-excitation of the Cy5, and by reducing the detector gain for the caveosome channel to 705, the crosstalk from the DNA could more or less be ignored. This was not the case with chitosan.

The settings used in these crosstalk experiment are more or less identical to those used in the main experiment (Table 4.1). Therefore, emission from chitosan when cross excited with 543nm HeNe laser was observed (seen as dimmer structures in Figure 4.19A, identical to the structures observed in Figure 4.19B). Sometimes, Cy5 emission were also observed, depending on the caveosomes detector gain and how intense the polyplexes lumps

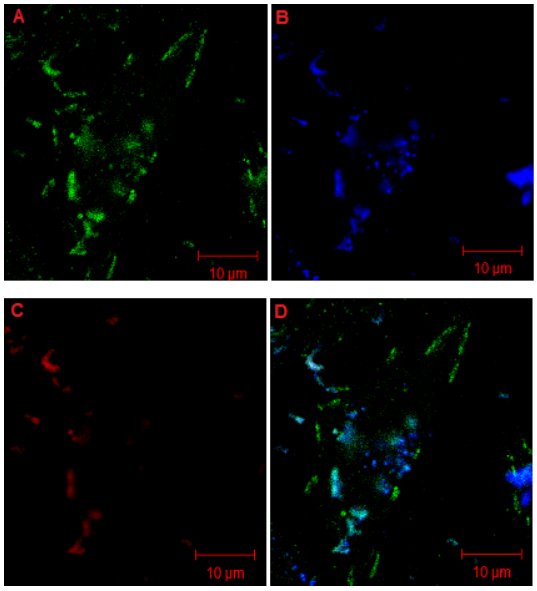

Figure 4.19: CLSM image of a cell showing cross talk between Alexa 488, Alexa 555 and Cy5. Caveosome channel (A), chitosan channel (B), DNA channel (C) and combined image (D)

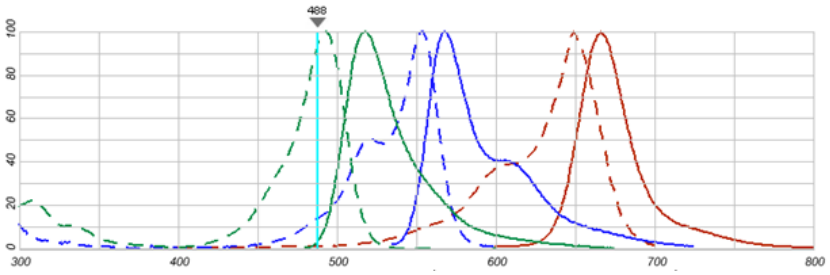

Figure 4.20: Excitation and emission spectra of Alexa 488, Alexa 555 and Cy5. Alexa 488 (green), Alexa 555 (blue) and Cy5 (red). Excitation are represented with broken lines while emission spectra are represented with straight line. Alexa 488 is excited around 488nm and emits around 518nm wavelength. Alexa 555 is excited at 555nm and emits around the 568nm wavelength. Cy5 is excited at 649nm and emits around 666nm wavelength.

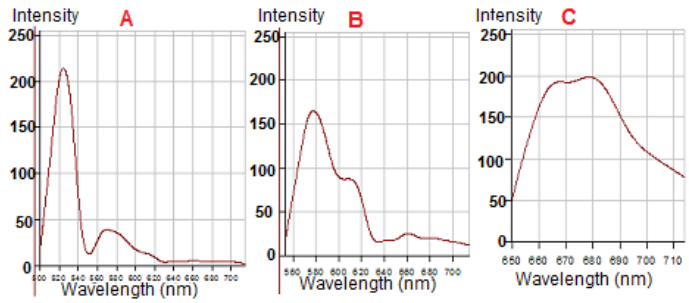

Figure 4.21: Emission spectra of the three dyes used in the experiment. The emission spectra of the dyes were derived from lambda series. Alexa 488 (A), Alexa 555 (B) and Cy5 (C).

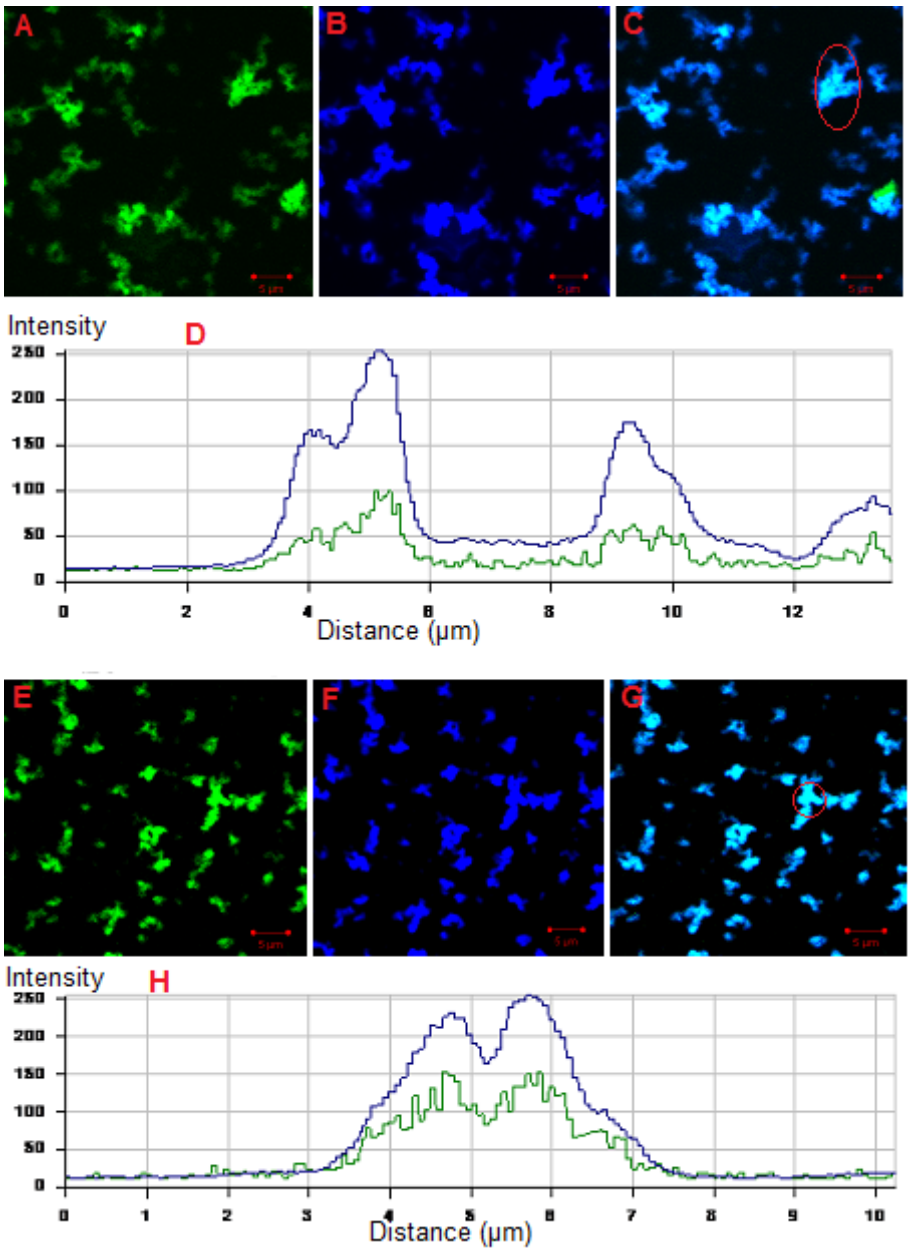

Figure 4.22: Images of the emission of cross-excited chitosan (green) with the 543nm HeNe laser (100% effect) recorded in the caveosomes channel (BP 565-615nm) (A,E). Images of the emission of Alexa 488-labelled chitosan (blue), excited with the 488nm Argon laser line (1% effect) and recorded in the chitosan channel (BP 500-550nm) (B,F). Merged images (C,G). Detector gain settings were 500 for chitosan channel (A,E) and 705 (B) or 785 (F) for the caveosomes channels. The intensity profiles across some polyplexes lumps are shown (D and H, blue line: chitosan channel, green line: caveosomes channel). Circles encloses ROI used to plot the intensity profile.

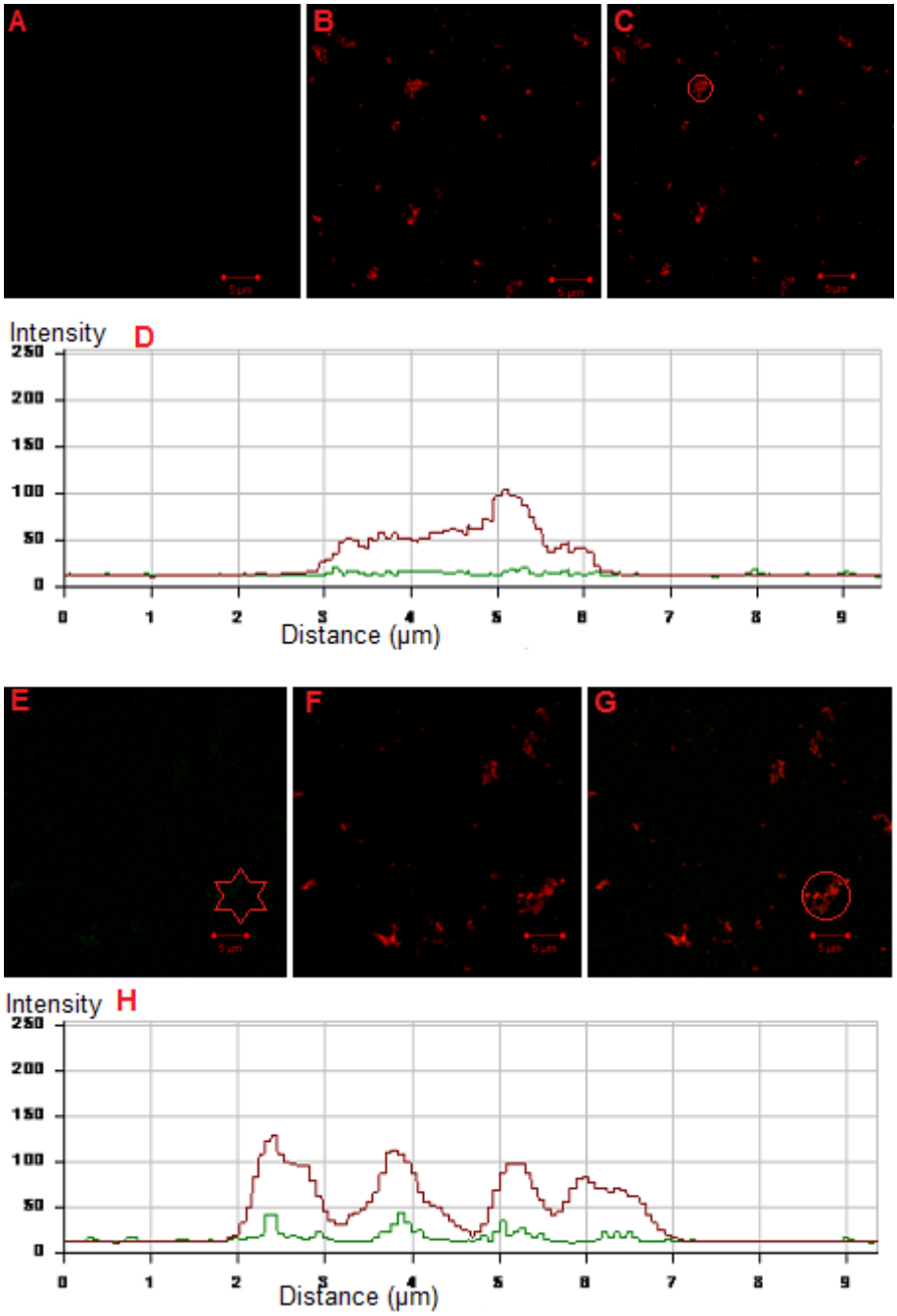

Figure 4.23: Images of the emission of cross-excited DNA (green) with the 543nm HeNe laser (1% effect) recorded in the caveosome channel (BP 565-615nm) (A,E). Images of the emission of the Cy5-labelled DNA (red), excited with the 633nm HeNe laser (2% effect) and recorded in the DNA channel (BP 654-704nm) (B,F). Merged images (C,G). Detector gain settings were 500 for the DNA channel (B,F) and 705 (A) or 785 (B) for the caveosome channel. The intensity profiles across some polyplexes lumps are shown (D and H, red line: DNA channel, green line: caveosome channel). Circles encloses ROI used to generate intensity profile.

Table 4.1: CLSM settings for acquisition of images

CLSM parameters	Alexa 488	Alexa 555	Cy5
Laser effect	1%	100%	2%
Detector gain	500	750	500

fluorescence.

A major problem here is the degree of labelling and aggregation of the polyplexes, causing very intense emission despite the low laser effect used. Likewise, the weak emission from Alexa555-sAb add to the problem. This imbalance in fluorophore excitation/emission will be discuss more in chapter 5.

Due to the crosstalk, images acquired were post processed by linear unmixing. Linear unmixing separates fluorescence detected by each channel using the emission spectra such as those shown in Figure 4.21, derived from lambda stacks (see appendix; lambda stacks).

Limited time available for this work could not allow linear unmixing to be carried out on all slides. Here unmixed images of HeLa cells incubated for 3 hours in polyplexes (either SBTCO or LCO polyplexes) is presented. In order to demonstrate colocalisation analysis, these unmixed images (Figure 4.24 and Figure 4.25) were analysed using the colocalisation plugin in imageJ .

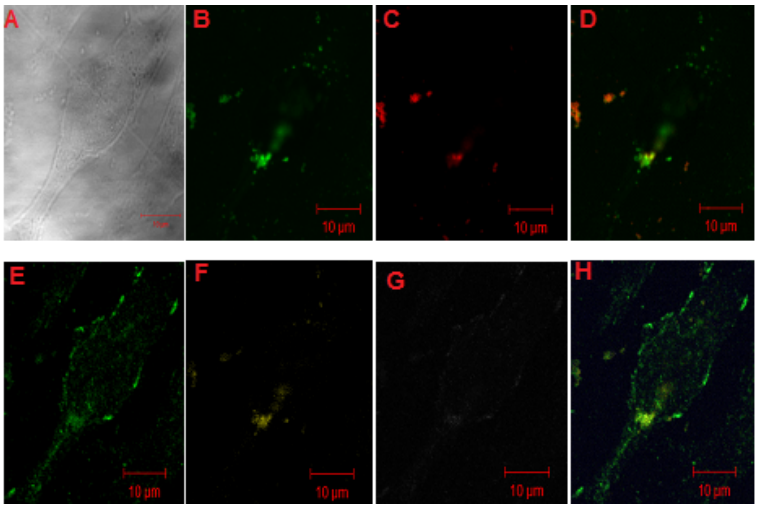

Figure 4.24: Images of HeLa cells incubated for 3 hours with SBTCO polyplexes before and after linear unmixing. DIC image (A), chitosan image before unmixing (B), DNA image before unmixing (C), combine image before unmixing (D), caveosome image after unmixing (E), chitosan image after unmixing (F), DNA image after unmixing (G) and combine image after unmixing (H). Chitosan (blue), DNA (red) and caveosome (green).

In HeLa cells incubated for 3 hours in SBTCO polyplexes, the unmixed images confirms

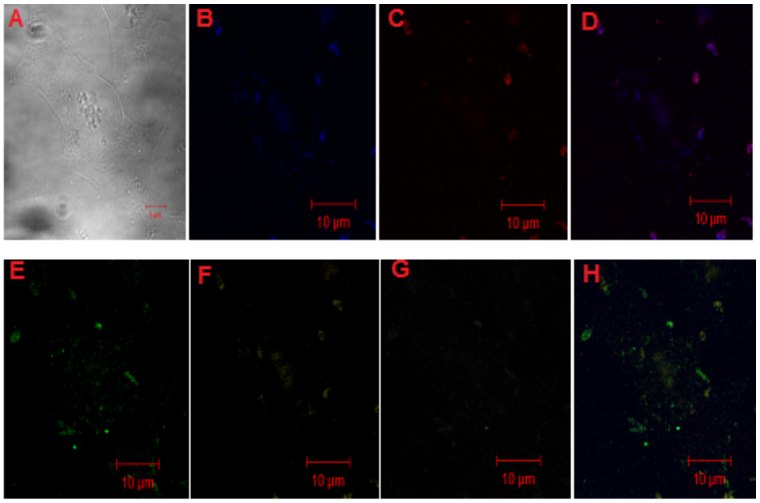

Figure 4.25: Images of HeLa cells incubated for 3 hours with LCO polyplexes before and after linear unmixing. DIC image (A), chitosan image before unmixing (B), DNA image before unmixing (C), combine image before unmixing (D), caveosome image after unmixing (E), chitosan image after unmixing (F), DNA image after unmixing (G) and combine image after unmixing (H). Chitosan (blue), DNA (red) and caveosome (green).

that caveosome were more, likewise the intracellular DNA (Figure 4.24) than their LCO incubated cell counterpart (Figure 4.25). The effect of linear unmixing, separating overlapping dyes can be seen when the images with crosstalk (Figure 4.24B-D and Figure 4.25B-D) are compare with unmixed images (Figure 4.24E-H and Figure 4.25E-H).

In HeLa cells incubated with either SBTCO and LCO polyplexes for 3 hours, the polyplexes colocalises with the caveosome, likewise, the caveosomes colocalises with polyplexes (Table 4.2), although the amount that colocalised differs between the two (Figure 4.26). Caveosome colocalised more with polyplexes (M_1) than polyplexes with caveosomes (M_2) (Table 4.2). In LCO polyplexes incubated cells, few polyplexes and few caveosomes were observed. In contrast, there were many polyplexes and caveosomes which were colocalised in SBTCO polyplexes incubated cells (Figure 4.26). In summary, more colocalised regions between polyplexes and caveosomes were located in the SBTCO polyplexes incubated cells than LCO polyplexes incubated cells as shown in Figure 4.26.

Table 4.2: Pearson's and Mander's coefficient of colocalisation at 3 hours period of incubation of Hela cells with polyplexes

	R_r	M_1	M_2
SBTCO polyplexes incubated cells	0.50 ± 0.16	1.00 ± 0.00	0.80 ± 0.11
LCO polyplexes incubated cells	0.50 ± 0.15	0.99 ± 0.01	0.80 ± 0.09

R_r = Pearson's coefficient, M_1 = colocalisation of caveosome with polyplexes and M_2 = colocalisation of polyplexes with with caveosomes. 5-6 cells were analysed. Images used were unmixed, 2D and non-deconvoluted.

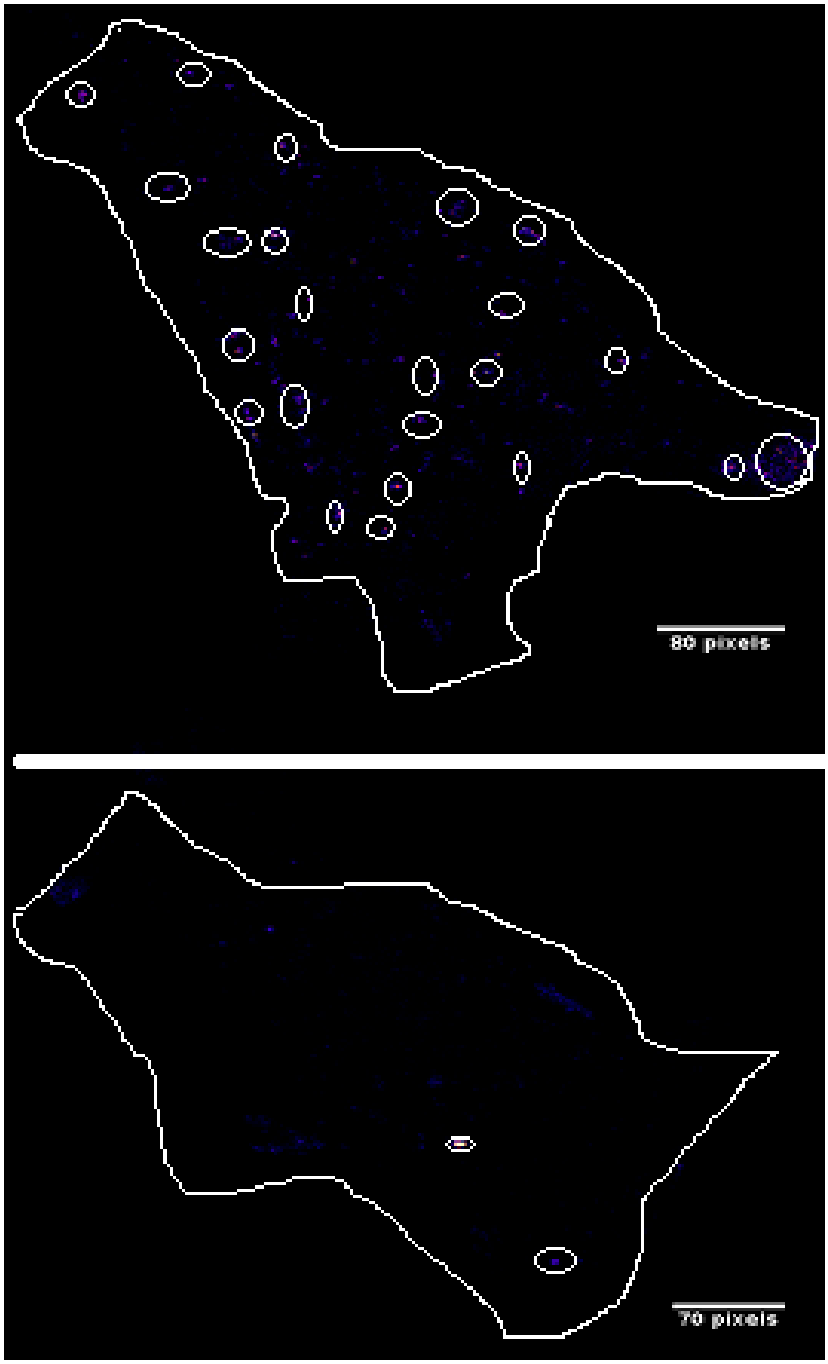

Figure 4.26: Colocalisation between polyplexes and caveosomes. Colocalisation between SBTCO polyplexes and caveosome (A). Colocalisation between LCO polyplexes and caveosome (B). Caveosome (blue), DNA (red) and colocalisation (purple). Both SBTCO and LCO polyplexes colocalised with caveosomes at 3 hours incubation period in HeLa cells. There were many polyplexes and caveosomes which were colocalised in SBTCO polyplexes incubated cells as described by the circle enclosure (A). In LCO polyplexes incubated cells, few polyplexes and few caveosomes were observes, the colocalised regions are enclosed in a circle (B).

Chapter 5

Discussion

Understanding intracellular processing of gene vectors will help to improve vector design in gene therapy. Chitosan nanoparticles have been previously identified as safe and non toxic gene vector [37]. LCO and SBTCO chitosan have been shown to adequately pack DNA, balancing between complexation and intracellular unpacking [13]. However, the transfection efficacies of these two chitosans differs considerably with the level of transgene expression higher for SBTCO compared to LCO [2, 4]. SBTCO has been recently reported to be taken up solely by CvME while LCO uses both CME and CvME (unpublished). This was verified using endocytosis pathways inhibitors specific for the two endocytotic pathways [38], and suggests that difference in transfection may be as a result of difference in intracellular processing pathway of the two polyplexes [38].

In the present study, the CvME was studied. An immunostaining protocol for detection of cav was established. Polyplexes of SBTCO seemed to trigger the formation of more caveosomes than did LCO polyplexes. Both SBTCO and LCO polyplexes were localised in the caveosomes at 3 hours incubation period, though the amount localised differ between the two polyplexes. SBTCO polyplexes localised, were more than the LCO polyplexes localised in the caveosomes.

5.1 Caveolae are stable membrane microdomain which are released by CTB

Cav are present in caveolae membrane domain of the cell [39]. Since the caveosomes were the organelle to be stained, the caveolae must be released from the membrane, thus cells were incubated with CTB known to bind GM1 receptor in the caveolae [26]. Prior

to incubation with CTB, only caveolae membrane domain were seen (Figure 4.1A). The incubation with CTB triggered formation and release of caveolar vesicle into the cell (Figure 4.1B) which suggested that caveolae are immobile membrane domains which need to be triggered in order to be release into the cell [20, 26, 40]. Immobility of the caveolae has been reported earlier [41, 42]. Considering the secretory pathway of cav, after synthesis in the endoplasmic reticulum, they are transported to the membrane where they are immobile. Deurs et al. [42] specified the calculated mobile fraction of caveolar to be 5-20% . This indicates that on insertion of cav into the cell membrane after synthesis via mobile vesicles from trans golgi network (TGN), they become trapped and immobilised in the caveolae [42].

The localisation of CTB intracellularly (Figure 4.1J and K) and it colocalisation with caveosomes (image overlaying) as shown in Figure 4.2 suggests CTB to be present in the caveosomes. Localisation of CTB in the caveosomes have been reported earlier [42, 43].

5.2 Optimising the concentration of primary and secondary antibody to labelled caveosome

In order to identify caveosome and be able to localise polyplexes in them (colocalisation), caveosomes were immunostained using pAb and Alexa555-sAb. The pAb binds to cav, and has been reported to be used for labelling cav [11]. Optimisation of caveosomes staining was carried out by testing different antibody combinations (Figure 4.1C-G). Concentration higher than the optimal generates non specific binding while those lower either produces no or too low fluorescence signal. Combination of $5\mu g/ml$ pAb with $5\mu g/ml$ Alexa555-sAb gave the best labelling (Figure 4.1B and C). This concentration was the best, probably due to balancing between pAb and Alexa555-sAb thereby avoiding non specific binding [31].

When concentration of pAb was higher than $5\mu g/ml$, non-specific binding of the antibody was observed. This type of non-specific binding of antibodies at high concentration of antibodies has been reported by Rogers et al. [44]. The non-specific binding in the images acquired with higher pAb concentration suggested that the concentration of the pAb be lowered. Several factors could be responsible for non specific binding of antibody of which thiol groups have been implicated [44]. Low fluorescence intensity when lower concentration of antibodies were used, suggested that the concentration of antibody should be increased. The good images acquired after staining with $5\mu g/ml$ pAb and $5\mu g/ml$ Alexa555-sAb (Figure 4.1B and C) showed this combination as the best.

It is worth discussing that the more extensive the washing, the less the non-specific binding observed. When the sample slide were washed mildly three times for 5 minutes, a lot of non-specific binding of antibodies were observed in the images (Figure 4.1J). The washing steps were changed into an extensive one carried out for 5 minutes twice, while the third washing was carried out on a shaker for 2 hours. These washing were carried out after each antibody labelling. The elimination of non- specific binding from the images suggested

that the washing steps removed more non-specific binding of antibodies, therefore, the mild washing was replaced by the extensive washing steps.

Blocking of potential binding site for secondary antibody which are not cav was an essential part of the optimisation procedure. Goat serum was used to block Alexa555-sAb and its effectiveness by the reduction of non-specific binding suggested it was good hence other blocking protein were not tried. Non-specific binding of antibody can also be block by casein, bovine serum albumin (BSA), milk etc. [45].

5.3 TOTO-3 washed out because it is an intercalating dye

In order to be able to visualise DNA and localise them in the cells, they have to be label. Binding mode of dyes is one of the important properties of dyes in terms of their applications in the analysis of nucleic acids and imaging. DNA used in this experiment was labelled with TOTO-3 at the start. TOTO-3 is useful in the detection of DNA. It is fluorescently stable and has a substantially higher sensitivity compare to some other known dyes [46, 47]. The dimeric forms of cyanine dyes are useful because they have higher binding affinity. Dimerisation is expected to reduce diffusion compared to their monomer counterpart.

Confocal images of cells incubated with TOTO-3 labelled DNA show that TOTO-3 smeared out in the whole cell after the extensive washing steps. This smearing increased with increasing time of washing (Figure 4.5). The smearing was because TOTO-3 intercalate between the DNA (reversible inclusion of molecule between the DNA). Intercalating dyes are generally aromatic cations with planar structures that insert between stacked base pairs in the DNA duplex [47]. A disadvantage of the dimeric forms of cyanine dyes is their high charge which makes their dissociation rates quite sensitive to ionic strength [46]. Intercalating dyes are not well bound to the nucleic acid unlike their covalent bounded counterparts such as Cy5.

Eriksson et al. [46] have compared intercalators and groove binding cyanine dye and found that intercalators dissociate faster than there groove binding partner [46]. This washing away of the dye suggested the change of DNA staining dye. Therefore, Cy5 was used to replace TOTO-3, and this eliminated the problem of smearing out of dye (Figure 4.6).

5.4 SBTCO polyplexes are protected from degradation in the cells

In this work polyplexes were shown to enter cytoplasm within the first 15 minutes of incubation; the intracellular polyplexes increases with time of incubation. With the knowledge

that SBTCO polyplexes are mainly taken up via the CvME and that LCO polyplexes are taken up via both CvME and CME (unpublished), analysing the intracellular DNA and caveosome of the cells will give more insight into the intracellular processing of these polyplexes.

5.4.1 SBTCO delivers higher DNA into the intracellular compartment

The intracellular DNA content analysed qualitatively (Figure 4.8 - Figure 4.13) and quantitatively (Figure 4.14A) suggested that the cellular uptake of DNA transported by the SBTCO was higher than that of LCO which could account for the high transfection by SBTCO reported by Sabina et al. [4]. DNA uptake was time dependent and the intracellular amount increased with increase in time of incubation.

Since LCO polyplexes are taken up by both CME and CvME (unpublished) and CME is constitutive in mammalian cells [6, 16], it might be expected of LCO polyplexes incubated cells to have higher intracellular DNA. In contrast, it was SBTCO polyplexes incubated cells that had higher intracellular DNA number. For all incubation times, DNA uptake by SBTCO polyplexes incubated cells were higher than DNA uptake in LCO polyplexes incubated cells. The difference in the DNA ($p < 0.05$) at 15 minutes and 1 hour between the SBTCO and LCO polyplexes incubated cells (Figure 4.14A) suggested that most LCO are taken up via CME, thereby leading to the endosomal degradation of DNA, and that the DNA level observed in LCO polyplexes incubated cells could be a result of those taken up via CvME.

At 3 hours incubation, the amount of intracellular DNA, transported by both polyplexes were not significantly different, which suggested that there has been some exchange of the LCO polyplexes in the degradative endosome with the non degradative caveosome. This suggested that at this time, LCO polyplexes were also located in the caveosomes which could protect the DNA. The transfer of LCO polyplexes into the caveosome could be regarded as intracellular re-targeting of the LCO polyplexes from the endosomes into the caveosomes. This re-targeting has been reported earlier [48, 49], while link between CvME and CME has been reported by Smith et al. [50]. Another explanation for the statistical insignificance at 3 hours incubation is the large SD between the values of intracellular DNA recorded.

Figure 4.14B and C shows that the volume of DNA transported by SBTCO were higher than the volume of DNA transported by LCO polyplexes which was significant at 3 hours of incubation. This increase in volume suggested aggregation of DNA transported by SBTCO, which could be due to the Cy5 cyanine dye used for labelling DNA. This type of aggregations by Cy5 has been reported by Reitan et al. [13]. It is well known that self-assembly in polar solutions is a common property of cyanine dyes and it is a frequently encountered phenomenon in dye chemistry. It is due to strong intermolecular van der Waals-like attractive forces between the molecules. Also, it has been reported earlier that cyanine dyes could undergo self-aggregation in aqueous media which was ascribed to the planarity of their structure [51].

In all cell analysed, amount of intracellular chitosan exceeds the DNA. This was observed in greater extent in SBTCO polyplexes incubated cells than in LCO polyplexes incubated cells. This high free chitosan ratio to polyplexes had been reported earlier [13]. It is as a result of high A/P ratio (1:5) SBTCO polyplexes used. Small amount of SBTCO was reported to be needed to complexes DNA, hence the rest existed as free chitosan [13]. In most cases the DNA do not colocalise with the SBTCO (Image overlaying), only few were observed to colocalise (Figure 4.8 - Figure 4.13). This indicates there were more free DNA particles than in complexe form, thereby confirming the ability of SBTCO to unpack intracellularly so as to ensure transfection [4].

5.4.2 SBTCO polyplexes triggers caveosome formation

CvME has been described to be more promising to gene therapy than CME, because it might mediate a non degradative intracellular processing via caveosomes [25]. It is importance to analyse the caveosome inside the cells to compare the ability of the two polyplexes to triggers caveosomes formation. The higher number of caveosomes dots in SBTCO polyplexes incubated cells for 3 hours (Figure 4.15) compared to LCO polyplexes incubated cells, suggested that SBTCO polyplexes triggered caveolae release from the membrane domain, causing an increase in number of caveosome. To confirm the qualitative analysis, quantitation of the caveosomes as shown in Figure 4.16A, confirmed that SBTCO triggered higher number of caveosomes than LCO polyplexes. This reaffirm that SBTCO polyplexes takes the CvME pathway as observed earlier (unpublished). Also, it reaffirm that SBTCO polyplexes are able to activate the release of caveolae from the membrane domain, leading to caveolar vesicle formation which fuses with the caveosomes. Stimulation of release and internalisation of caveolae has been reported [42].

Comparing the caveosome number inside cells (Figure 4.16A), it is worth noting that decrease in caveosome number in the LCO polyplexes incubated cells suggests that caveosomes are not the major organelles involved in intracellular processing of LCO polyplexes. Furthermore, it suggested that LCO might prefer other pathway, for processing. The higher number of caveosomes in cells incubated with SBTCO polyplexes indicates that SBTCO polyplexes are more linked to caveosomes than LCO polyplexes. Comparing Figure 4.14A and Figure 4.16A, increase intracellular DNA in LCO polyplexes incubated cells and low number of caveosomes recorded in them further suggested CvME is not LCO polyplexes major pathway of uptake and processing. Furthermore, the increase in DNA recorded in these LCO polyplexes incubated cells might be a result of uptake via other pathway such as CME (a constitutive endocytic pathway in the mammalian cell) [6, 16].

Figure 4.16B and C suggested that the caveosomes triggered by the SBTCO polyplexes, increase in size with time of incubation which suggested that the SBTCO polyplexes are stored in this caveosome organelle before being transferred further to their final destination. The use of caveosome for storage of cargo has been reported [20].

5.5 Approaches to avoiding or solving the problem of crosstalk

To compare LCO and SBTCO in relation to caveosomes using colocalisation analysis, three dyes were used for labelling. As was shown in Figure 4.19, chitosan was recorded in the caveosome channel, due to crosstalk. This crosstalk makes the post imaging processing difficult if the images are to be analysed for colocalisation. Understanding how to solve crosstalk problem is important because crosstalk is a common problem in multidye imaging. Here are suggestions to how crosstalk can be avoided or eliminated:

5.5.1 Choice of dyes

The crosstalk experienced in this work was a result of the overlap of excitation and emission spectra of the three dyes used (Figure 4.20). The excitation spectra overlapped a bit, and especially the emission spectra for Alexa 488 and Alexa 555. It is very important in a multicolour experiment to choose dyes where the excitation spectra do not overlap, to selectively excite only one fluorochrome at a time. In this work, the 543 nm HeNe laser intended for the excitation of the Alexa 555-labelled caveosomes, also excited the Alexa 488-labelled chitosan and the Cy5-labelled DNA. The excitation spectra of Alexa 488 is at a minimum at 543 nm, as illustrated by the normalised curves in Figure 4.20, but scanning with the intense green laser (100% effect), excited the concentrated polyplexes lumps of Alexa 488 and also the concentrated Cy5-labelled DNA. It is of great importance to apply dyes in concentrations that yield similar intensities when scanning with similar laser powers. This was not the case in the work presented here (Table 4.1).

It is important to study the emission spectra of the dyes used in the experiment. They should not overlap too closely. This is the case for the tail of the Alexa 488 spectrum and the Alexa 555 spectrum (Figure 4.21). When cross-excited with the green laser, the emission of the Alexa 488 was recorded in the caveosome channel. The filter used was the BP 565 - 615, which picks up the peak of the Alexa 555 emission, but unfortunately also the tail at higher wavelength of the Alexa 488 emission. Furthermore, cross-excitation of Cy5 causes some bleed-through of the Cy5 signal into this Alexa 555 channel.

5.5.2 Imaging reference samples

Before any experimental work involving multilabeling is carried out, cross-excitation and bleed-through should be tested on reference samples of single-labelled specimen, with conditions (concentration of dye, laser effect, detector gain etc.) identical to those to be used for the multicolour experiment. The concentrations of the dyes and the image acquisition settings should be tune in order to eliminate noise and crosstalk. If cross-excitation and bleed-through cannot be avoided, lambda stacks can be acquired that can be used for linear unmixing.

5.5.3 Imaging strategies

Images can be acquire by two methods, which are;

Sequential detection

It is highly recommended to perform sequential acquisitions, exciting one fluorophore at a time using the optimal laser line and switching between the detectors [36]. The disadvantage of sequential detection includes longer image acquisition times and errors generated from the misalignment of the system from image to image. Sequential detection might not be applicable to living cells imaging because the cells might change position [52].

Parallel detection

Here, fixed single or multiple frequency excitation is applied with several detector and with several fluorophore. If the laser effects, the detector gains, and the band pass filters are chosen carefully, crosstalk can be avoided. The advantage of parallel detection is that it is much faster and dynamic processes can be measured with high precision [52].

5.5.4 Post-processing of the images

Channel unmixing

In cases where crosstalk is observed after imaging, a way to go on with analysis is by doing spectral unmixing of the multilabelled images. Spectral unmixing is a simple mathematical operation that was originally developed for satellite imaging [36]. By spectral unmixing, it is possible to enhance the chromatic resolution of fluorescence microscopy.

The simplest way of doing spectral unmixing is by experimentally determining the crosstalk factor for a given optical configuration and using this factor to derive corrected values for each pixel [36]. To unmix the spectra of fluorophore with strongly overlapping spectra, as in this experiment, the contributions of the different dyes to the overall signal were determined. The lambda series of the caveosomes were unmixed by fitting the observed spectrum in each pixel to a mix of the reference spectra of Alexa 488, Alexa 555 and the background spectrum. A least squares fitting approach was used to estimate the proportion or weight of the individual reference spectra. The lambda series were then splitted into images of the different dyes, corresponding to caveosomes, the chitosan and the background. A more detailed insight into the calculations is shown in the appendix (linear unmixing). It worth noting that the unmixed image of caveosome, chitosan and DNA in Figure 4.24

and Figure 4.25 look like ordinary images, this suggested that the unmixing algorithm was good.

5.6 Colocalisation analysis

Location and physiological function of proteins are related. localisation of polyplexes in the caveosomes can be use to probe polyplexes uptake and intracellular trafficking. The degree of colocalisation is measured by comparing the equivalent pixel positions in the acquired images. To perform colocalisation analysis, factors such as the quality and reliability of markers, acquisition microscope and techniques, labelling techniques and knowledge of the three dimensional organisation of the cell must be considered [36]. Colocalisation cannot be carried out with images with crosstalk, this will give a false positive result, hence all images with crosstalk must be unmix (image post processing).

Although colocalisation analysis was carried out on HeLa cells incubated for 3 hours only, the analysis can explain what happens to the polyplexes and where they were at 3 hours incubation period. Colocalisation between intracellular SBTCO and LCO polyplexes and caveosomes at 3 hours incubation period suggested that both polyplexes were located in the caveosomes at this time (Table 4.2), though, of different amount (Figure 4.26).

Few caveosome located in the LCO polyplexes incubated cells, confirmed that LCO triggers less caveosome and that LCO polyplexes have a preferred pathway of which CME has been implicated. In this laboratory, it has been reported that LCO polyplexes were localised in early endosome at 15 minutes, 1 hour and 3 hours incubation period (unpublished). Early endosomes are formed when clathrin coat depolymerises. They can fuse with each other or with other preexisting endosomes to form late endosomes that further fuse with lysosomes [6].

The large amount of intracellular SBTCO polyplexes which colocalises with caveosomes in SBTCO polyplexes incubated cells confirmed that SBTCO are solely processed via the CvME thereby being protected from the hydrolytic degradation in the endosomes. In contrast, the low amount of LCO polyplexes in LCO polyplexes incubated cells (Figure 4.26B) suggested that most LCO polyplexes has been degraded in the endosome.

In summary, the colocalisation analysis at 3 hours incubation period confirmed SBTCO to be processed solely by CvME pathway, and that they are localised in the caveosome at this period of incubation. It also confirmed that LCO preferred intracellular processing pathway is not CvME.

Chapter 6

Conclusion and Suggestion for future work

6.1 Conclusion

The aim of this work was achieved. An immunostaining protocol for detection of caveolin was established. Comparison between the two polyplexes LCO and SBTCO chitosans in relation to CvME was carried out. Polyplexes of SBTCO seemed to trigger the formation of more caveosomes than did LCO polyplexes. Both SBTCO and LCO polyplexes were localised in the caveosomes at 3 hours incubation period, though of different amount. SBTCO polyplexes located in the caveosomes were higher than LCO polyplexes located in the caveosomes.

These findings shows that SBTCO polyplexes delivers more DNA into the cell and it intracellular processing is solely by CvME compare to LCO polyplexes. Further more, it shows that SBTCO is protected from the degradative endosome and might therefore be an efficient and good tool to deliver therapeutic DNA.

6.2 Suggestion for future work

Since the colocalisation quantification of the polyplexes with the caveosome could not be carried out at all incubation time, due to time limitation, it would be of interest to colocalise these polyplexes with the caveosome at other incubation time (15 minutes and 1 hour). This will help to ascertain the location of the polyplexes at the different incubation time.

Colocalisation analysis will be more easier if the dyes to be used in labelling the polyplexes and the caveosomes are chosen so that their spectra do not overlap. Furthermore, the labelling must be carried out so that equal fluorescence intensity would be produce by the dyes. This will help to avoid imbalance among the labels. Likewise, it will help to avoid the problem of crosstalk, thereby, linear unmixing might not be needed.

It might be of interest to try another antibody which binds proteins related to cav. Antibody such as those binding polymerase I and transcript release factor (PTRF-cavin) also known as cav-p60 or cavin could be use. Furthermore, antibodies with higher affinity for caveolin can be use, this will reduce the amount of the dye needed to achieve optimal fluorescence. Therefore, image acquisition will be achieve with low laser effect thereby eliminating the problem of crosstalk. Lastly, organelles such as GA and ER can be label and localisation of SBTCO polyplexes in them could be quantified. This will further show where SBTCO polyplexes are located after leaving caveosomes.

Bibliography

[1] Won Y.Y., Sharma R. and Konieczny S.F. *Missing pieces in understanding the intracellular trafficking of polycation/DNA complexes*. Journal of control release, 139:88-93 (2009).

[2] Malmo J., Vårum K.M. and Strand S.P. *Effect of chitosan chain architecture on gene delivery : comparism of self branched and linear chitosan*. Biomacromolecules, 12(3):721-729 (2011).

[3] Mao S., Sun W. and Kissel T. *Chitosan-based formulations for delivery of DNA and siRNA*. Advanced drug delivery reviews, 62 (1):12-27 (2010).

[4] Strand S.P., Issa M.M., Christensen B.E., Vårum K.M., and Artursson P. *Tailoring chitosans for gene delivery: Novel self branched glycosylated chitosan oligomers with improved functional properties*. Biomacromolecules, 9:3268-3276 (2008).

[5] Akhtar S. *Non-viral cancer gene therapy: beyond delivery*. Gene therapy, 13:739-740 (2006).

[6] Khalil I.A., Kogure K., Akita H. and Harashima H. *Uptake pathways and subsequent intracellular trafficking in nonviral gene delivery.* Pharmacological reviews, 58(1):32-45 (2006).

[7] Elouahabi A. and Ruysschaert J.M. *Formation and intracellular trafficking of lipoplexes and polyplexes*. Molecular therapy, 11:36-347 (2005).

[8] Martin B., Sainlos M., Aissaoui A., Oudrhiri N., Hauchecorne M., Vigneron J.P., Lehn J.M. and Lehn P. *The design of cationic lipids for gene delivery*. Current pharmaceutical design, 11: 375-394 (2005).

[9] Ogris M. and Wagner E. *Tumor-targeted gene transfer with DNA polyplexes*. Somatic cell and molecular genetics, 27(1-6):85-95 (2002).

[10] Severian D. *Polysaccharides. Structural Diversity and Functional Versatility*. Mercel Dekker publisher 2nd edition chapter 26, page 625-642 (2005).

[11] Chiu Y.L., Ho Y.C., Peng S.F., Ke C.J., Chen K.J., Mi F.L. and Sung H.W. *The characteristics, cellular uptake and intracellular trafficking of nanoparticle made of hydrophobically -modified chitosan*. Journal of control release, 146:152-159 (2010).

[12] Strand S.P., Lelu S., Reitan N.K., Davies C.de L., Artursson P. and Vårum K.M. *Molecular design of chitosan gene delivery systems with an optimised balance between polyplexe stability and polyplexe unpacking*. Biomaterials, 31:975-987 (2010).

[13] Reitan N.K., Maurstad G., Davies C.de L. and Strand S.P. *Characterizing DNA condensation by structurally different chitosans of variable gene transfer efficacy*. Biomacromolecules, 10:1508-1515 (2009).

[14] Schnitzer J.E. *Caveolae: from basic trafficking mechanism to targeting transcytosis for tissue-specific drug and gene delivery in vivo*. Advance drug delivery reviews, 49:265-280 (2001).

[15] Kirkham M. and Parton R.G. *Clathrin-independent endocytosis: new insights into caveolae and non caeolar lipid raft carriers*. Biochimica et biophysica acta, 1745:273-286 (2005).

[16] Conner S.D. and Sandra L.S. *Regulated portals of entry into the cells*. Nature, 422: 37-44 (2003).

[17] Albert B., Johnson A., Lewis J., Raff M., Robert K. and Walter P. *Molecular biology of cell*. Garlang science, 5th edition page 749-812 (2008).

[18] Iversen T.G., Skotland T. and Sandvig K. *Endocytosis and intracellular transport of nanoparticles : present knowledge and need for future studies*. Nantoday, 6(2): 176-185 (2011).

[19] Luzio P.J., Parkinson M.D.J., Gray S.R. and Bright N.A. *The delivery of endocytosed cargo to lysosomes*. Biochemical society transaction, 37:1019-1021 (2009).

[20] Pietiäinen V.M., Marjomäki V., Heino J. and Hyypiä T. *Viral entry, lipid rafts and caveosomes*. Annals of medicine, 37:394-403 (2005).

[21] Parton R.G., Richards A.A. *Lipid Rafts and Caveolae as Portals for Endocytosis: New Insights and Common Mechanisms*. Traffic, 4:724-738 (2003).

[22] Quest A.F.G., Leyton L. and Parraga M. *Caveolins, caveolae and lipid rafts in cellular transport, signalling and disease*. Biochemistry and cell Biology, 82:129-144 (2004).

[23] Hansen C.G. and Nichols B.J. *Exploring the caves: cavins, caveolins and caveolae*. Trends in cell biology, 20(4):177-186 (2010).

[24] Carver L.A. and Schnitzer J.E. *Caveolae: minning little caves for new cancer targets*. Nature reviews; cancer, 3:571-581 (2003).

[25] Pelkmans L. and Helenius A. *Endocytosis via caveolae*. Traffic, 3:311-320 (2002).

[26] Tarrago-Trani M.T. and Storrie B. *Alternate routes for drug delivery to cell interior*. Advance drug delivery review, 59(8):782-797 (2007).

[27] Pelkmans L. *Secrets of caveolae- and lipid raft-mediated endocytosis revealed by mammalian viruses*. Biochimica et biophysica acta, 1746:295-304 (2005).

[28] Gumbleton M., Hollins A.J, Omidi Y., Campbell L. and Taylor G. *Targeting caveolar for vessicle transport*. Journal of control release, 87:139-151 (2003).

[29] Stan R.V. *Structure of caeolae*. Biochimica et biophysica acta, 1746:334-348 (2005).

[30] Head B.P. and Insel P.A. *Do caveolins regulate cells by actions outside of caveolae?* Trends in cell biology, 17(2):51-57 (2007).

[31] Kindt T.J., Osborne B.A. and Goldsby R.A. *Kuby immunology*. 6th edition, page 975-987 (2007).

[32] Berg K., Folini M., Prasmickaite L., Selbo P.K., Bonsted A., Engesæter B.Ø.N., Weyergang A., Dietze A., Mælandsmo G.M., Wagner E., Norum O.J. and Høgset A. *Photochemical internalisation: a new tool for drug delivery*. Current pharmaceutical biotechnology, (8):362-372 (2007).

[33] Lakowicz J.R. *Principles of Fluorescence Spectroscopy*. Springer publisher 4th edition, chapter 1, page 1-8 (2006)

[34] Dieing T., Hollricher O. and Toporski J. *Confocal raman microscopy*. Springer, page 3-4 (2011).

[35] Oldfield, R. *Encyclopedia of life science*. John wiley and sons, Ltd., pages 1-4 (2001).

[36] Bolte S. and Cordelières F.P. *A guided tour into subcellular colocalization analysis in light microscopy*. Journal of microscopy, 224:213-232 (2006).

[37] Lai W.F. and Lin M.C.M. *Nucleic acid delivery with chitosan and its derivates*. Journal of control release, 134:158-168 (2009).

[38] Folasire O.S. *Mechanism of chitosan-DNA nanoparticle endocytosis*. Master project for department of biotechnology, Norwegian University of Science and Technology, (2010).

[39] Parton R.G. and Simons K. *The multiple faces of caveolae*. Nature reviews; Molecular cell biology, 8: 185-194 (2007).

[40] Fielding C.J. *Lipid rafts and caveolae, from membrane biophysics to cell biology*. Wiley-VCH Verlag GmbH and Co.KGaA, pages 5-30 (2006).

[41] Thomsen P., Roepstorff K., Stahlhut M. and Deurs B.V. *Caveolae are highly immobile plasma membrane microdomains, which are not involved in constitutive endocytic trafficking*. Molecular biology of cell, 13:238-250(2002).

[42] Deurs B.V., Roepstorff K., Hommelgaard A.M. and Sandvig K. *Caveolae: anchored, multifunctional platforms in the lipid ocean*. Trends in cell biology, 13(2):92-100 (2003).

[43] Nichols B.J. *A distinct class of endosome mediates clathrin-independent endocytosis to the Golgi complex*. Nature cell biology, 4:374-378 (2002).

[44] Rogers A.B., Cormier K.S. and Fox J.G. *Thiol-reactive compounds prevent nono specific antibody binding in immunohistochemistry*. Laboratory investigation, 86:526-533 (2006).

[45] Ramos-Vara J.A. *Technical Aspects of Immunohistochemistry*. Veterinary pathology, 42:405-426 (2005).

[46] Eriksson M, Karlsson H.J., Westman G and Björn Å. *Groove-binding unsymmetrical cyanine dyes for staining of DNA: dissociation rates in free solution and electrophoresis gels*. Nucleic acid research, 31(21):6235-6242 (2003).

[47] Deligeorgiev T.G., Kaloyanova S. and Vaquero J.J. *Intercalating cyanine dyes for nucleic acid detection*. Recent patent on materials, 2:1-26 (2009).

[48] Parton R.G. *Caveolae meet endosomes: a stable relationship*. Developmental cell, 7(4):458-460 (2004).

[49] Pelkans L., Bürli T., Zerial M. and Helenius A. *Caveolin-stabilized membrane domains as multifunctional transport and sorting devices in the endocytic membrane traffick*. Cell, 118:767-780 (2004).

[50] Smith J.L., Campos S.K., Wandinger -Ness A. and Ozbun M.A. *Caveolin-1- dependent infectious entry of human papillomavirus type 31 in human keratinocytes proceeds to the endosomal pathway for the pH- dependent uncoating*. Journal of virology, 82(19):9505-9512 (2008).

[51] Biver T., Biasi A.D., Secco F., Venturini M. and Yarmoluk S. *Cyanine Dyes as Intercalating Agents: Kinetic and Thermodynamic Studies on the DNA/Cyan40 and DNA/CCyan2 Systems*. Biophysical journal, 89:374-383 (2005).

[52] Ahammer H., DeVaney T.T.J., Hartbauer N. and Tritthart H.A. *Cross-talk reduction in confocal images of dual fluorescence labelled cell spheroids*. Micron, 30:309-317 (1999).

[53] Hiraoka Y., shimi T. and Haraguchi T. *Multispectra imaging fluorescence microscopy for living cells*. Cell structure and function, 27:367-374 (2002).

Chapter 7

Appendix

7.1 Linear unmixing

$$I(\lambda) = A.R(\lambda) \tag{7.1}$$

$$I(\lambda) = A_1.R_1(\lambda) + A_2.R_2(\lambda).....A_i.R_i(\lambda) \tag{7.2}$$

$$I(\lambda) = \sum A_i.R_i(\lambda) \tag{7.3}$$

or

$$I = \sum A.R(\lambda) \tag{7.4}$$

Applying the inverse least square fitting approach:

$$\frac{\delta}{\delta A_i} \sum_i [I(\lambda_i) - \sum_i A_i R_i(\lambda_i)]^2 = 0 \tag{7.5}$$

therefore

$$\sum_i R_i(\lambda_i)[I(\lambda_i) - \sum_i A_i R_i(\lambda_i)] = 0 \tag{7.6}$$

Where I = signal in each pixel

$I(\lambda)$ = mean spectrum

$R(\lambda)$ = reference spectrum

A = weight (contribution of each fluorophore) [53].

7.2 Colocalisation coefficients

Pearson's coefficient

$$R_r = \frac{\sum(S1_i - S1_{aver}).(S2_i - S2_{aver})}{\sqrt{\sum(S1_i - S1_{aver})^2.\sum(S2_i - S2_{aver})^2}} \tag{7.7}$$

Where R_r: Pearson's coefficient, S_1: Signal intensity of pixels in first channel, S_2: signal intensity in the second channel, $S1_{aver}$and $S2_{aver}$: average intensity of first and second channels respectively.

colocalisation coefficient M_1 ***and*** M_2

$$M_1 = \frac{\sum(S1)_{i,coloc}}{\sum(S1)_i} \tag{7.8}$$

$$M_2 = \frac{\sum(S2)_{i,coloc}}{\sum(S2)_i} \tag{7.9}$$

where M_1 is colocalisation of the first channel and M_2 colocalisation of the second channel $(S1)_{i,coloc} = (S1)_i$ if $(S2)_i$ is within threshold defined by ROI.

$S1_{i,coloc} = 0$ if $S2_i$ if outside the threshold levels.

$S1_{i,coloc} = S2_i$ if $S1_i$ is within threshold.

$S2_{i,coloc} = 0$ if $S1_i$ is outside ROI

$(S2)_{i,coloc}$= $(S2)_i$ if $(S1)_i > 0$ [36].

Overlap coefficient

$$R = \frac{\sum S1_i.S2_i}{\sqrt{\sum(S1_i)^2.\sum(S2_i)^2}} \tag{7.10}$$

Overlap coefficient K_1 ***and*** K_2

$$K_1 = \frac{\sum S1_i.S2_i}{\sum(S1_i)^2} \tag{7.11}$$

$$K_2 = \frac{\sum S1_i.S2_i}{\sum(S2_i)^2} \tag{7.12}$$

where K_1 = overlapping coefficient K_1

and K_2 = overlapping coefficient K_2

colocalisation coefficient m_1 ***and*** m_2

$$m_1 = \frac{\sum(S1)_{i,coloc}}{\sum(S1)_i} \tag{7.13}$$

$$m_2 = \frac{\sum(S2)_{i,coloc}}{\sum(S2)_i} \tag{7.14}$$

where where colocalisation for each colour channel m_1 and m_2

$(S1)_{i,coloc}$= $(S1)_i$ if $(S2)_i > 0$

$(S2)_{i,coloc}$= $(S2)_i$ if $(S1)_i > 0$ [36].

7.3 Lambda stacks

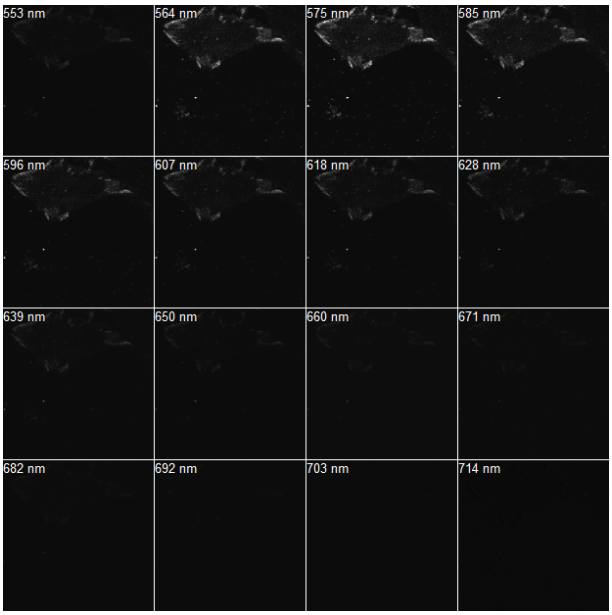

Figure 7.1: lambda stack of Alexa 555 labelled caveosome. It describes the emission data from a series of small wavelength bands. Lambda stack are generally used in plotting emission spectra of dyes which are used in channel unmixing. This lambda stack is between 553nm and 714nm with 10-11nm interval.

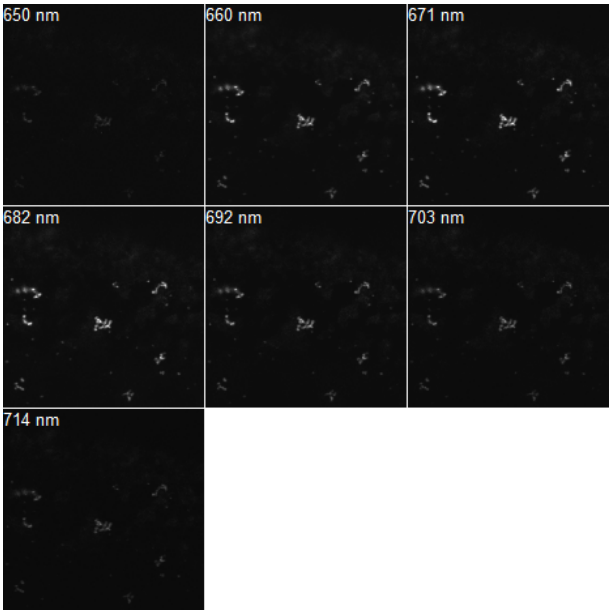

Figure 7.2: The lambda image of the Cy5 labelled DNA. This stacks are used to generate the emission spectra of Cy5. This lambda stack is between 650nm and 714nm with 10-11nm interval.

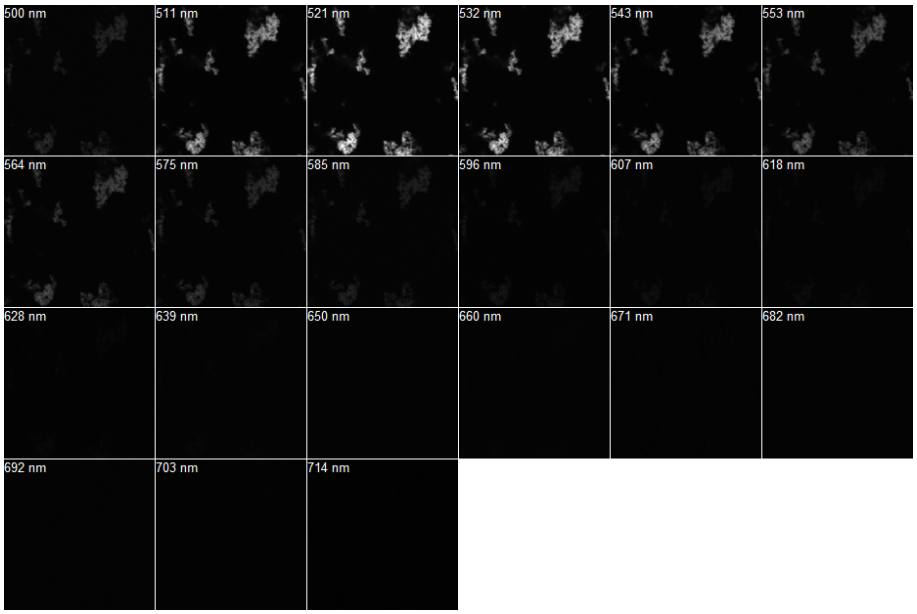

Figure 7.3: The lambda image of Alexa 488 labelled chitosan. The lambda stack is between 500nm and 714nm with 10-11nm interval.